SIAM J. APPLIED DYNAMICAL SYSTEMS
Vol. 0, No. 0, pp. 000–000

On Differential Equations with Codimension-n Discontinuity Sets*

Peter L. Varkonyi† and Mate Antali‡

Abstract. This paper investigates fundamental properties of a new class of dynamical systems, which are everywhere smooth except for a codimension-n discontinuity manifold with an arbitrary positive integer n. Such systems emerge naturally in modeling the motion of bodies with spatial point contacts as well as with finite contact surfaces under dry friction. As a special case, the investigated class includes Filippov systems ($n = 1$) as well as the recently introduced extended Filippov systems ($n = 2$). Trajectories reaching the discontinuity manifold are studied in detail, and new types of pathological behavior are uncovered, in systems where the local dynamics around the discontinuity manifold involves polycycles or strange attractors. The concept of crossing and sliding dynamics is extended for this type of system. The results are illustrated by several examples.

Key words. nonsmooth, Filippov, discontinuity, sliding, friction

AMS subject classifications. 34A36, 34C05, 37N05, 70F40

DOI. 10.1137/20M1360773

1. Introduction.

The field of *piecewise smooth systems* is a rapidly developing area of dynamical systems theory, which can be used for modeling many physical, engineering, or biological systems. An important subclass of these systems is often called *Filippov systems*, where the vector field has a jump on a certain *switching manifold* in the phase space. The concept of these vector fields with the switching behavior was founded mainly by Filippov [11], Utkin [35], and Teixeira [33, 34]. A detailed overview of the area and further references can be found in [7] and [17].

Mechanics of contacting bodies is an important application of discontinuous dynamics (see [24] for an overview). The main motivation of the present analysis is mechanical systems with *dry friction*, especially when it is modeled by the *Coulomb friction model*. Consider a planar problem with a rigid block slipping on a rough surface, which is a usual application example of piecewise smooth systems. Then, the one-dimensional description of the velocity state (slipping left or right) leads to a piecewise smooth Filippov system, where the static *sticking* state is related to the switching surface in the phase space.

However, in more complicated cases, dry friction *goes beyond* the area of piecewise smooth systems. In the case of planar friction with a single contact point, the switching surface is a

*Received by the editors August 18, 2020; accepted for publication (in revised form) by T. Seara May 24, 2021; published electronically DATE.
https://doi.org/10.1137/20M1360773

Funding: The research of the first author was supported by the National Research, Development, and Innovation Office under grant K124002. The research of the second author was supported by the Hungarian Academy of Sciences in the Premium Postdoctoral Fellowship Programme under grant PPD2018-014/2018.

†Department of Mechanics, Materials and Structures, Budapest University of Technology and Economics, Budapest, H-1111, Hungary (vpeter@mit.bme.hu).

‡Department of Applied Mechanics, Budapest University of Technology and Economics, Budapest, H-1111, Hungary (antali@mm.bme.hu).

codimension-1 *discontinuity set*. When we analyze the spatial problem of a slipping block with two velocity components, the vector field has a discontinuity in a *codimension*-2 discontinuity set. Then, the phase space shows a rather different picture from switching between distinct regions. For the analysis of such *extended Filippov systems*, the concepts of piecewise smooth systems were generalized in [2], and the results were applied to spatial mechanical problems in [3]. Systems with higher codimensional discontinuity emerge when local deformations and friction over a finite contact area are considered. Adding *drilling friction* (normal friction torque) to the friction model creates a *codimension*-3 discontinuity, which can be seen from the results in [23] and [21]. Moreover, adding the *creep effect* of rolling elastic bodies [18] introduces discontinuous coupling with further state variables which can lead to a reduced system with a *codimension*-5 discontinuity set.

Our motivation is to describe the class of vector fields, which covers all types of discontinuities mentioned above. For that, we consider a vector field which is smooth everywhere except in a codimension-n submanifold of the phase space. Then, we use the concepts and terminology of piecewise smooth systems [7, 17]. In the literature, different approaches such as complementary problems and set-valued force laws [23, 13, 5, 37] are used for the analysis of the discontinuities induced by spatial friction. Further formulations can be found in [4], and [28]. A detailed comparison of these approaches is a task left for future work. We note, however, that a clear benefit of our approach is uncovering special objects such as *limit directions* and *limit cones*, which determine the qualitative behavior of the vector field at the discontinuity set.

A wide variety of discontinuity-induced dynamics is known to emerge at the *intersection* of several discontinuity sets, which arise, for example, in mechanical systems with multiple contacts. The intersection of k codimension-1 discontinuities was analyzed in detail in [8, 16, 26, 19]. This situation results in a *non-isolated* codimension-k discontinuity set, which requires a different approach from that of the present paper. Some basic results about the intersection of codimension-2 discontinuity sets can be found in [1], but a detailed analysis of this topic is beyond the scope of this paper.

In the literature, analysis of piecewise smooth systems is often based on *regularization*, the *blow-up method*, or the combination of the two (see [32, 25] or the recent works [29, 6, 30]). These methods often lead to multiscale dynamical systems (see [22] for an overview), analyzed in the context of Fenichel theory [10]. In this paper, we use a basic approach of polar blow-up around the codimension-n discontinuity set in order to investigate local dynamics in a close neighborhood of the discontinuity set. In addition, initial steps are taken to define and study *sliding* dynamics along the discontinuity. Other questions of sliding dynamics and bifurcations induced by codimension-n discontinuities are questions left for future work.

The structure of the paper is the following. In section 2, the analyzed class of vector fields is introduced, and the basic concepts are formulated. The central part of the paper is section 3, where the qualitative behavior of the system is analyzed focusing on the trajectories which are connected to the discontinuity set. In section 4, several examples illustrate the main findings. In section 5, the concepts of *sliding* and *crossing* regions are extended to this type of systems using Filippov's convex method, and sliding dynamics within the discontinuity manifold is also defined.

2. Vector fields with codimension-n discontinuities. In this section, we introduce codimension-n discontinuities of vector fields and the necessary mathematical formulation for the subsequent analysis.

2.1. Problem statement. Consider the differential equation

$$\dot{\mathbf{x}} = \mathbf{F}(\mathbf{x}), \tag{2.1}$$

where $\mathbf{x} = (x_1, x_2 \dots x_m) \in \mathbb{R}^m$ and $\mathbf{F} = (F_1, F_2, \dots F_m)$ is an $\mathbb{R}^m \to \mathbb{R}^m$ vector field. A dot means differentiation with respect to time t, and the explicit time dependence $\mathbf{x}(t)$ is not denoted except when it is necessary. We assume that the vector field has a codimension-n discontinuity in the subspace Σ spanned by the coordinates $x_1 \dots x_n$. That is, we consider the *discontinuity set*

$$\Sigma = \{\mathbf{x} \in \mathbb{R}^m : x_1 = x_2 = \dots x_n = 0\}. \tag{2.2}$$

Assume that $\mathbf{F}$ is smooth everywhere in $\mathbb{R}^m \setminus \Sigma$. Even though $\mathbf{F}$ is not defined in Σ, it is assumed that in all points $\bar{\mathbf{x}} \in \Sigma$ the limit

$$\mathbf{F}^\star(\bar{\mathbf{x}}, \mathbf{v}) := \lim_{\epsilon \searrow 0} \mathbf{F}(\bar{\mathbf{x}} + \epsilon \mathbf{v}) \tag{2.3}$$

exists for any vector $\mathbf{v} \in \mathbb{R}^m$ not tangential to Σ, and the limit depends smoothly on $\mathbf{v}$ and $\bar{\mathbf{x}}$.

Our aim is to understand how the trajectories of the differential equation (2.1) behave locally in a small neighborhood of Σ. In particular, we will focus in sections 2–4 on trajectories that start or end at a point $\bar{\mathbf{x}} \in \Sigma$.

Note that the description could be extended from the state space $\mathbb{R}^m$ to an m dimensional smooth manifold, and the discontinuity Σ would be an $m-n$ dimensional smooth submanifold. By mapping the manifolds locally to linear spaces, the formulation (2.1)–(2.2) can be used for a local analysis without loss of generality.

2.2. On the classification and terminology of nonsmooth systems. The classification and terminology of nonsmooth dynamical systems vary slightly in the different works in the literature. In this subsection, we give a brief overview of the classification from different aspects and show the location of the analyzed system (2.1) in these categories.

- **The *codimension* of the discontinuity:** The term *piecewise smooth systems* is used for a large class of nonsmooth dynamical systems—including maps and vector fields—where the system is smooth everywhere in the phase space except on some *codimension*-1 discontinuity sets (manifolds) [7, 17, 24]. In some cases, the discontinuity set can be called a *switching surface* separating some *smooth* regions of dynamics. The system (2.1) is a piecewise smooth system for $n = 1$. However, it is beyond the class of piecewise smooth systems for $n > 1$ because a higher codimensional discontinuity appears. The case $n = 2$ was presented by the second author in [3], and the general $n \geq 1$ case is analyzed in the present paper. Note that in piecewise smooth systems, higher codimensional discontinuities can appear at the *intersection* of several codimension-1 discontinuity sets [8, 16, 17]. However, the behavior of those intersecting discontinuities is rather different from the *isolated* higher codimensional discontinuities of (2.1). Here, we cannot speak about *switching* behavior or being smooth in distinct regions: In the $n > 1$ case of (2.1), the system is smooth everywhere around the higher codimensional discontinuity set.

- **The *type* of the discontinuity:** On page 73 of [7], we can find the definition of *degree of smoothness* (DS) of piecewise smooth systems with the following consequence: The case DS $= 0$ corresponds to the *hybrid* systems where the trajectory has a jump at the discontinuity set. (A typical physical source of these systems is impact between rigid bodies.) In the DS $= 1$ case, the *vector field* has a jump at the discontinuity. These vector fields are often called *Filippov systems* (see, e.g., [7, p. 75]). In the case DS ≥ 2, the vector field is $\mathcal{C}^{\mathrm{DS}-1}$ continuous at the discontinuity set, systems which are usually called *piecewise smooth continuous* systems. In the case $n = 1$ of (2.1), the discontinuity Σ has a *uniform* degree of smoothness 1, except if (2.3) is independent of the direction $\mathbf{v}$. Thus, this is the case of Filippov systems. If $n > 1$, (2.1) ensures a similar type of discontinuity. This was the reason that the case $n = 2$ was called an *extended Filippov system* in [3].
- **The behaviour *outside* and *inside* the discontinuity:** Part of the analysis of nonsmooth systems is related to the analysis of the sections of the trajectories in the smooth regions of the phase space *outside* the discontinuity set. A further task is to connect the sections of the trajectories *through* or even *inside* the discontinuity set. For the latter case, the dynamics can be sometimes extended to the discontinuity set, which is called *sliding dynamics*. For this, *additional information* or assumptions are needed about the dynamical system. The simplest possibility is to create a *convex combination* of the directional limits of the vector field, which is usually called *Filippov's convex method*. In addition to the convex method being *linear* in some switching variables, there are *nonlinear* ways to connect the boundaries of the discontinuity (see, e.g., [35, 6, 29, 17]. Most of the present paper is devoted to the analysis of trajectories *in the vicinity* of the discontinuity set Σ (section 2 to 4), where we still do not have to include the convex or nonconvex assumptions in the discontinuity. In section 5, a brief analysis is shown by using a *convex combination* similar to Filippov's convex method. The detailed analysis of sliding and crossing dynamics by considering the nonlinear sliding dynamics is beyond the scope of the paper.

2.3. Appropriate transformations for the analysis. In this subsection, we carry out some transformations of the system (2.1) to reach a form of the equations appropriate for the subsequent analysis.

2.3.1. Decomposition to tangential and orthogonal parts. Let us first separate the state variable $\mathbf{x}$ into parts *orthogonal* to Σ (denoted by $\mathbf{x}_o$) and *tangential* to Σ (denoted by $\mathbf{x}_t$). That is,

$$\mathbf{x} = \mathbf{x}_o + \mathbf{x}_t = (x_1, \dots x_n, 0, \dots 0) + (0, \dots 0, x_{n+1}, \dots x_m). \tag{2.4}$$

The vector field is written in the form $\mathbf{F} = \mathbf{F}_o + \mathbf{F}_t$ such that the dynamics becomes $\dot{\mathbf{x}}_o = \mathbf{F}_o(\mathbf{x})$ and $\dot{\mathbf{x}}_t = \mathbf{F}_t(\mathbf{x})$.

2.3.2. Introducing spherical variables. In the next step, let us rewrite the orthogonal variable $\mathbf{x}_o$ in a similar way to that of polar and spherical coordinates. We consider

$$\mathbf{x}_o = r\mathbf{w}, \tag{2.5}$$

where $r = \|\mathbf{x}_o\| = \sqrt{\sum_{i=1}^n x_i^2}$ is the *distance* of $\mathbf{x}$ from the discontinuity Σ, and $\mathbf{w} = \mathbf{x}_o/\|\mathbf{x}_o\| = (w_1, \dots w_n, 0, \dots 0)$ is the unit vector showing the *direction* of $\mathbf{x}$ around Σ. Note that throughout the paper, $\|\mathbf{a}\| = \sqrt{\mathbf{a}^\top \mathbf{a}}$ denotes the usual 2-norm of a vector, $\mathbf{a} \in \mathbb{R}^m$, and $^\top$ denotes the transpose of a vector or a linear mapping. Note that this set of variables is redundant, and the solutions preserve the constraint

$$\|\mathbf{w}\| = \sqrt{\sum_{i=1}^n w_i^2} = 1. \tag{2.6}$$

Thus, $\mathbf{w}$ is located on the unit sphere $\mathbb{S}^{n-1} \subset \mathbb{R}^m$. By the transformation (2.4)–(2.5), the triplet $(r, \mathbf{w}, \mathbf{x}_t) \in \mathbb{R}^+ \times \mathbb{S}^{n-1} \times \mathbb{R}^{m-n}$ is mapped to $\mathbf{x} \in \mathbb{R}^m \setminus \Sigma$. That is, we can identify the two sets, $\mathbf{x} = (r, \mathbf{w}, \mathbf{x}_t)$, and we use the two notations interchangeably.

The orthogonal part of the vector field can be written in the form

$$\mathbf{F}_o = R(\mathbf{x})\mathbf{w} + \mathbf{V}(\mathbf{x}), \tag{2.7}$$

where

$$R(\mathbf{x}) = \mathbf{w}^\top \mathbf{F}_o(\mathbf{x}) \tag{2.8}$$

is the *radial* part of the vector field and

$$\mathbf{V}(\mathbf{x}) = \mathbf{F}_o - \mathbf{w}^\top \mathbf{F}_o(\mathbf{x})\mathbf{w} \tag{2.9}$$

is the *circumferential* part. By these notations, we recast (2.1) as

$$\dot{r} = R(r, \mathbf{w}, \mathbf{x}_t), \tag{2.10}$$
$$\dot{\mathbf{w}} = \mathbf{V}(r, \mathbf{w}, \mathbf{x}_t)/r, \tag{2.11}$$
$$\dot{\mathbf{x}}_t = \mathbf{F}_t(r, \mathbf{w}, \mathbf{x}_t). \tag{2.12}$$

Note that due to the smooth dependence required in (2.3), the functions R, $\mathbf{V}$, and $\mathbf{F}_t$ are smooth in the set $\mathbb{R}^+ \times \mathbb{S}^{n-1} \times \mathbb{R}^{m-n} \ni (r, \mathbf{w}, \mathbf{x}_t)$, and the discontinuity is located at $r = 0$.

2.3.3. Limit of the vector field at the discontinuity. The assumed continuity properties of $\mathbf{F}$ imply that the functions R, $\mathbf{V}$, and $\mathbf{F}_t$ have well-defined limit values

$$R^\star(\mathbf{w}, \mathbf{x}_t) := \lim_{r \searrow 0} R(r, \mathbf{w}, \mathbf{x}_t), \tag{2.13}$$
$$\mathbf{V}^\star(\mathbf{w}, \mathbf{x}_t) := \lim_{r \searrow 0} \mathbf{V}(r, \mathbf{w}, \mathbf{x}_t), \tag{2.14}$$
$$\mathbf{F}_t^\star(\mathbf{w}, \mathbf{x}_t) := \lim_{r \searrow 0} \mathbf{F}_t(r, \mathbf{w}, \mathbf{x}_t), \tag{2.15}$$

which are smooth functions in $\mathbf{w}$ and $\mathbf{x}_t$.

Our goal is to analyze trajectories which either start from or end at a point $\mathbf{x} = \bar{\mathbf{x}} = (0, \mathbf{0}, \bar{\mathbf{x}}_t) \in \Sigma$ of the discontinuity set. Thus, we analyze an approximate dynamics in the vicinity of a point $\bar{\mathbf{x}}$. By using the limits (2.13)–(2.15), we can approximate (2.10)–(2.12) by the *asymptotic* dynamics

$$\dot{r} = R^\star(\mathbf{w}, \bar{\mathbf{x}}_t), \tag{2.16}$$

$$\dot{\mathbf{w}} = \mathbf{V}^\star(\mathbf{w}, \bar{\mathbf{x}}_t)/r, \tag{2.17}$$

$$\dot{\mathbf{x}}_t = \mathbf{F}_t^\star(\mathbf{w}, \bar{\mathbf{x}}_t). \tag{2.18}$$

By using the decomposition $\mathbf{x} = r\mathbf{w} + \mathbf{x}_t$, the approximate dynamics in the original form (2.1) becomes

$$\dot{\mathbf{x}} = \mathbf{F}^\star(\mathbf{x}) = R^\star(\mathbf{w}, \bar{\mathbf{x}}_t)\mathbf{w} + \mathbf{V}^\star(\mathbf{w}, \bar{\mathbf{x}}_t) + \mathbf{F}_t^\star(\mathbf{w}, \bar{\mathbf{x}}_t). \tag{2.19}$$

We will show later in subsection 3.3 that from the analysis of the asymptotic approximation (2.17)–(2.18), we can get information about the structure of the phase space of the full system (2.10)–(2.12), as well. Roughly speaking, we can think of the asymptotic dynamics as a leading-order approximation involving zeroth-order terms.

2.3.4. Time rescaling at the singularity.

The singularity associated with $r = 0$ is removed by a singular rescaling of time,

$$\frac{\mathrm{d}}{\mathrm{d}\tau} = r\frac{\mathrm{d}}{\mathrm{d}t}. \tag{2.20}$$

Then, (2.10)–(2.12) becomes

$$r' = rR(r, \mathbf{w}, \mathbf{x}_t), \tag{2.21}$$

$$\mathbf{w}' = \mathbf{V}(r, \mathbf{w}, \mathbf{x}_t), \tag{2.22}$$

$$\mathbf{x}_t' = r\mathbf{F}_t(r, \mathbf{w}, \mathbf{x}_t), \tag{2.23}$$

where the dash denotes derivation with respect to the new time variable τ. This transformation does not change the trajectories of the system.

If we extend the domain of the functions by using the limit values (2.13)–(2.15), then the system (2.21)–(2.23) is smooth in $(r, \mathbf{w}, \mathbf{x}_t) \in \mathbb{R}_{\geq 0} \times \mathbb{S}^{n-1} \times \mathbb{R}^{m-n}$, including $r = 0$. The region $r < 0$ is still excluded due to the restriction $r \geq 0$ of the spherical radial coordinate. Time rescaling (2.20) of the *asymptotic* dynamics (2.16)–(2.18) becomes

$$r' = rR^\star(\mathbf{w}, \bar{\mathbf{x}}_t), \tag{2.24}$$

$$\mathbf{w}' = \mathbf{V}^\star(\mathbf{w}, \bar{\mathbf{x}}_t), \tag{2.25}$$

$$\mathbf{x}_t' = r\mathbf{F}_t^\star(\mathbf{w}, \bar{\mathbf{x}}_t). \tag{2.26}$$

3. Analysis via multiple time scales.

In the vicinity of $r = 0$ located at the former discontinuity, the system (2.21)–(2.23) behaves as a *multiple time scale* dynamical system where $\mathbf{w}$ is a *fast* variable and r and $\mathbf{x}_t$ are *slow* variables.

In the approximated system (2.24)–(2.26), the fast dynamics of $\mathbf{w}$ fully decouples from the other two slow variables and (2.25) can be solved independently. (Note that $\bar{\mathbf{x}}_t$ is a fixed value.) First, we give a brief overview on possible types of fast dynamics (2.25). Then, the slow dynamics is investigated by taking into account the long-term behavior of the fast variables. Finally, we draw consequences to the qualitative behavior of the full system (2.21)–(2.23).

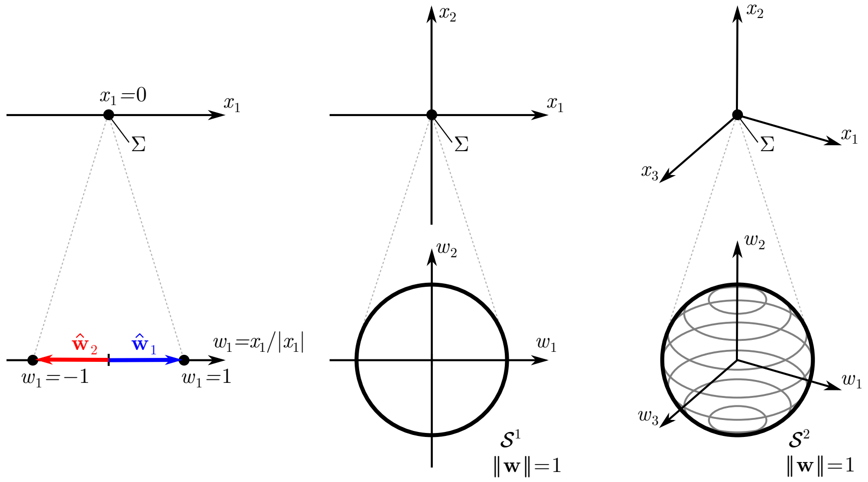

FIGURE 1. *Sketch of the phase space around the discontinuity for different values of the codimension n. Upper row: the sketch of the phase space projected onto the subspace of the orthogonal variables $\mathbf{x}_o$. In these projected graphs, the discontinuity is depicted as a point, which contains the other (tangential) variables $\mathbf{x}_t$. Bottom row: the subspace of the* fast dynamics *of* $\mathbf{w}$ *on a unit sphere $\mathcal{S}^{n-1}$. Left column: the codimension-*1 *case, corresponding to the (classical) Filippov systems. Here, the phase space of the fast dynamics consists of two discrete points corresponding to two trivial limit directions $\hat{\mathbf{w}}_1$ and $\hat{\mathbf{w}}_2$. Middle column: the codimension-*2 *case; the fast dynamics of* $\mathbf{w}$ *is located on a unit circle. Right column: the codimension-*3 *case; the fast dynamics of* $\mathbf{w}$ *is located on a unit sphere.*

3.1. Fast dynamics of w. The fast system (2.25) is a smooth dynamical system whose state space is the $n-1$ sphere $\mathbb{S}^{n-1} \subset \mathbb{R}^m$ of radius 1. As we will see in Section 3.2, the long-term behavior of the fast subsystem has a crucial role in the analysis of the slow dynamics. To that end, we briefly review classical results of dynamical systems theory [14] regarding the qualitatively different types of long-term behavior for low values of n:

- **Codimension-1 discontinuity, Filippov systems:** If $n = 1$, then the domain of the fast dynamics is two isolated fixed points $\hat{\mathbf{w}}_1 = (1, 0, \ldots 0)$ and $\hat{\mathbf{w}}_2 = (-1, 0, \ldots 0)$. That is, the dynamics of $\mathbf{w}$ is trivial, $\mathbf{w}(t) \equiv \hat{\mathbf{w}}_1$ or $\mathbf{w}(t) \equiv \hat{\mathbf{w}}_2$ as illustrated by the leftmost column of Figure 1. This is the well-known case of classical Filippov systems where the discontinuity manifold has two disconnected sides [7, 17].
- **Codimension-2 discontinuity, extended Filippov systems:** If $n = 2$, then the domain of (2.25) is the unit circle $\mathbb{S}^1$; see the middle column of Figure 1. This is the case of extended Filippov systems investigated in [2]. Trajectories of dynamical systems on circles always converge to fixed points forward and backward in time, or every trajectory is a periodic orbit covering the circle (if there are no fixed points).
- **Codimension-3 discontinuity**: If $n = 3$, then the domain of (2.25) is the unit sphere $\mathbb{S}^2$ (right column of Figure 1). According to the Poincaré–Bendixson theorem and its generalizations [27], modest regularity assumptions imply that trajectories converge to fixed points, limit cycles, or polycycles. Among these, the last one will result in subtle difficulties during the analysis of the induced slow dynamics, as explained in Section 3.2 and illustrated by Example 4.5 below.

- **Higher codimension cases**: If $n > 3$, then the domain is a unit hyper-sphere $\mathbb{S}^{n-1}$. Trajectories may have various qualitatively different types of behavior, including convergence to fixed points, periodic orbits, quasi-periodic orbits, polycycles, and strange attractors. As we will see in subsection 3.2, the first three types allow the use of averaging techniques to predict the slow dynamics; however, this is not the case for other types in general.

3.2. Slow dynamics of r. When the fast dynamics (2.25) of $\mathbf{w}$ approaches an invariant set presented in subsection 3.1, we want to analyze the dynamics of r according to (2.24). For this analysis, it is useful to introduce the rescaled radial variable $\rho = \log r$. If the solution $\mathbf{w}(\tau)$ is known from the fast dynamics (2.25), then the evolution of ρ is given by

$$\rho(\tau) - \rho(0) = \int_0^\tau \rho'(\eta)\mathrm{d}\eta = \int_0^\tau \frac{r'(\eta)}{r(\eta)}\mathrm{d}\eta = \int_0^\tau R^\star(\mathbf{w}(\eta), \bar{\mathbf{x}}_t)\mathrm{d}\eta. \tag{3.1}$$

The discontinuity set Σ is located at $r = 0$, which corresponds to $\rho = -\infty$. Thus, a trajectory tending to Σ in forward or backward time is characterized by $\lim_{\tau\to\pm\infty} \rho(\tau) = -\infty$, which leads to

$$\lim_{\tau\to\pm\infty} \int_0^\tau R^\star(\mathbf{w}(\eta), \bar{\mathbf{x}}_t)\mathrm{d}\eta = -\infty. \tag{3.2}$$

For each type of invariant set of $\mathbf{w}$ (see subsection 3.1), we can describe the radial dynamics by analyzing the integral (3.2).

3.2.1. Fixed points of w-limit directions of the system. We have seen that the fast dynamics often converges to a fixed point $\mathbf{w} = \hat{\mathbf{w}}$. Then, the analysis of (3.2) reduces to checking the sign of $R^\star(\hat{\mathbf{w}})$.

Definition 3.1. *Consider the fixed point $\hat{\mathbf{w}}$ of the circumferential dynamics satisfying $\mathbf{V}^\star(\hat{\mathbf{w}}, \bar{\mathbf{x}}_t) = \mathbf{0}$. Then, we call $\hat{\mathbf{w}}$ a* limit direction *of the system* (2.1) *at $\bar{\mathbf{x}}_t$. In the case $R^\star(\hat{\mathbf{w}}, \bar{\mathbf{x}}_t) < 0$ or $R^\star(\hat{\mathbf{w}}, \bar{\mathbf{x}}_t) > 0$, $\hat{\mathbf{w}}$ is called an* attracting *or a* repelling *limit direction, respectively.*

By using the term limit *direction*, we identify the point $\hat{\mathbf{w}} \in \mathbb{S}^{n-1} \subset \mathbb{R}^m$ and the half-line $\mathcal{L} : \mathbb{R}^+ \to \mathbb{R}^m$, $\mathcal{L}(\rho) = \bar{\mathbf{x}} + \rho\hat{\mathbf{w}}$. The concept of limit direction is depicted in the left column of Figure 2.

Theorem 3.2. *Consider an attracting limit direction $\hat{\mathbf{w}}$ at $\bar{\mathbf{x}} = \bar{\mathbf{x}}_t \in \Sigma$. Then, there exists a trajectory $\mathbf{x}(t)$ of* (2.19) *and $\hat{t} \in \mathbb{R}$ such as*

$$\lim_{t\nearrow\hat{t}} \mathbf{x}(t) = \bar{\mathbf{x}} \tag{3.3}$$

and

$$\lim_{t\nearrow\hat{t}} \mathbf{w}(t) = \hat{\mathbf{w}}(t). \tag{3.4}$$

Proof. Consider a trajectory $\mathbf{x}(\tau) = (r(\tau)), \mathbf{w}(\tau), \mathbf{x}_t(\tau))$ with a starting point $r(0) = r_0 = \exp\rho_0$; $\mathbf{w}(0) = \hat{\mathbf{w}}$; $\mathbf{x}_t(0) = \mathbf{x}_{t,0}$. Then, $\mathbf{w}(\tau) \equiv \hat{\mathbf{w}}$ according to Definition 3.1, and from

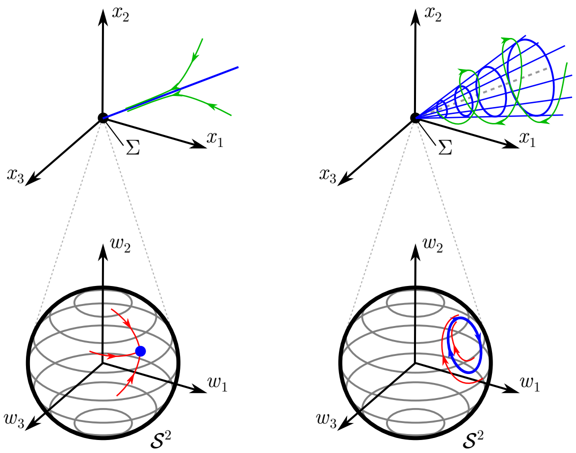

FIGURE 2. *Limit directions and limit cones at the discontinuity depicted in the codimension-3 case. The upper and lower rows show the phase space projected to the orthogonal subspace and the fast subspace, respectively, similarly to Figure 1. Left column: a* limit direction *is a characteristic direction in the (orthogonal) phase space and a fixed point in the fast subspace of* $\mathbf{w}$. *Right column: a* limit cone *is a conical-shaped organizing surface of trajectories in the orthogonal space, which corresponds to a limit cycle in the fast subspace of* $\mathbf{w}$.

(2.19), (3.4) is trivially satisfied for any time $\hat{t}$ until the discontinuity manifold is reached. The constant value $R^\star(\hat{\mathbf{w}}, \bar{\mathbf{x}}_t) < 0$ makes the integrand of (3.2) finite and negative, thus, $\lim_{\tau\to\infty} \rho(\tau) = -\infty$ corresponding to $r \to 0$. In particular, $\rho(\tau) = \rho_0 + R^\star(\hat{\mathbf{w}}, \bar{\mathbf{x}}_t)\tau$. Let $t(\tau)$ denote the time of the original time scale according to (2.20). By assuming $t(0) = 0$, the time $\hat{t}$ of reaching the discontinuity becomes

$$\begin{aligned}(3.5)\quad \hat{t} = \lim_{\tau\to\infty} t(\tau) &= \int_0^\infty \frac{\mathrm{d}t(\tau)}{\mathrm{d}\tau}\mathrm{d}\tau = \int_0^\infty r(\tau)\mathrm{d}\tau \\ &= \int_0^\infty \exp(\rho_0 + R^\star(\hat{\mathbf{w}}, \bar{\mathbf{x}}_t)\tau)\mathrm{d}\tau = \frac{-\exp(\rho_0)}{R^\star(\hat{\mathbf{w}}, \bar{\mathbf{x}}_t)} = \frac{-r_0}{R^\star(\hat{\mathbf{w}}, \bar{\mathbf{x}}_t)}.\end{aligned}$$

Then, (2.26) implies that by choosing

$$\mathbf{x}_{t,0} = \bar{\mathbf{x}}_t + \frac{r_0 \mathbf{F}_t^\star(\mathbf{w}, \bar{\mathbf{x}}_t)}{R^\star(\hat{\mathbf{w}}, \bar{\mathbf{x}}_t)},$$

the trajectory satisfies (3.3), which completes the proof. ■

A variant of Theorem 3.2 can be proposed for the repelling limit directions.

Theorem 3.3. *Consider a repelling limit direction* $\hat{\mathbf{w}}$ *at* $\bar{\mathbf{x}} = \bar{\mathbf{x}}_t \in \Sigma$. *Then, there exists a trajectory* $\mathbf{x}(t)$ *of* (2.19) *and* $\hat{t} \in \mathbb{R}$ *such as*

$$(3.6)\qquad \lim_{t\searrow\hat{t}} \mathbf{x}(t) = \bar{\mathbf{x}}, \qquad\qquad \lim_{t\searrow\hat{t}} \mathbf{w}(t) = \hat{\mathbf{w}}.$$

Proof. The proof is analogously to Theorem 3.2. ■

Theorems 3.2–3.3 are trivial in the case of $n = 1$ (Filippov systems) and they have been proved by [2] in the case of $n = 2$. The generalization to arbitrary n is a new contribution of this work.

There is an analogy between limit directions of a point $\bar{\mathbf{x}} \in \Sigma$ and the *eigenvectors* of a usual fixed point: both are organizing lines of trajectories approaching the critical point of the vector field. However, there are two fundamental differences:

- More accurately, the eigenvectors are lines (bidirectional), but the limit directions are half-lines (unidirectional).
- Along a usual eigenvector, the trajectories approach the equilibrium point *exponentially* (the convergence takes *infinite* time). Along a limit direction, the trajectories approach $\bar{\mathbf{x}}$ *faster than exponentially* (the convergence takes *finite* time).
- The number of eigenvectors cannot be higher than the dimension of the state space; there is, however, no such limitation for limit directions.

Note that by the time transformation (2.20), we effectively slow down the system in such a way that the convergence becomes exponential in the transformed time scale τ. (See the linear leading term of r in the radial dynamics (2.24).)

At the borderline case of $R^\star(\hat{\mathbf{w}}, \bar{\mathbf{x}}_t) = 0$ a *bifurcation* occurs between the attracting and repelling behavior. This bifurcation can be considered either a special subset of Σ satisfying $R^\star(\hat{\mathbf{w}}, \bar{\mathbf{x}}_t) = 0$ or a special property of a fixed $\bar{\mathbf{x}} \in \Sigma$ in the presence of varying system parameters. In the codimension-1 case of Filippov systems, this is called a *tangency point* (see [17, p. 50]), and the concept was extended to the codimension-2 case in [2]. General analysis of this bifurcation is beyond the scope of the present work. Now we just point out that the name *tangency* seems to be appropriate in the codimension-n description: If $\mathbf{V}(\hat{\mathbf{w}}, \bar{\mathbf{x}}_t) = 0$ and $R^\star(\hat{\mathbf{w}}, \bar{\mathbf{x}}_t) = 0$, then the approximate dynamics (2.24)–(2.26) gives that the vector field is *tangent* to the discontinuity set Σ at the selected point $\bar{\mathbf{x}}$ and at the direction $\hat{\mathbf{w}}$.

In the proof of Theorem 3.2, we constructed a *single* trivial trajectory at the fixed point $\hat{\mathbf{w}}$ of (2.25). According to the type of the fixed point, the limit directions can be categorized to get information about other trajectories satisfying (3.3)–(3.4).

Definition 3.4. *Consider a limit direction $\hat{\mathbf{w}}$ at $\bar{\mathbf{x}} = (0, \mathbf{0}, \bar{\mathbf{x}}_t) \in \Sigma$. Assume that $\hat{\mathbf{w}}$ is a hyperbolic fixed point of (2.25) with eigenvalues $\lambda_1 \dots \lambda_k$. The limit direction is called*

- dominant *if*

$$\min_{i \in 1 \dots k} R^\star(\hat{\mathbf{w}}, \bar{\mathbf{x}}_t) \mathrm{Re}\lambda_i > 0; \tag{3.7}$$

- isolated *if*

$$\max_{i \in 1 \dots k} R^\star(\hat{\mathbf{w}}, \bar{\mathbf{x}}_t) \mathrm{Re}\lambda_i < 0; \tag{3.8}$$

- saddle-type *if*

$$\min_{i \in 1 \dots k} R^\star(\hat{\mathbf{w}}, \bar{\mathbf{x}}_t) \mathrm{Re}\lambda_i \cdot \max_{i \in 1 \dots k} R^\star(\hat{\mathbf{w}}, \bar{\mathbf{x}}_t) \mathrm{Re}\lambda_i < 0. \tag{3.9}$$

In other words, a stable node or focus of (2.25) corresponds to an attracting-dominant or a repelling-isolated limit direction, an unstable node or focus corresponds to an attracting-isolated or repelling-dominant limit direction, and a saddle corresponds to a saddle-type limit direction.

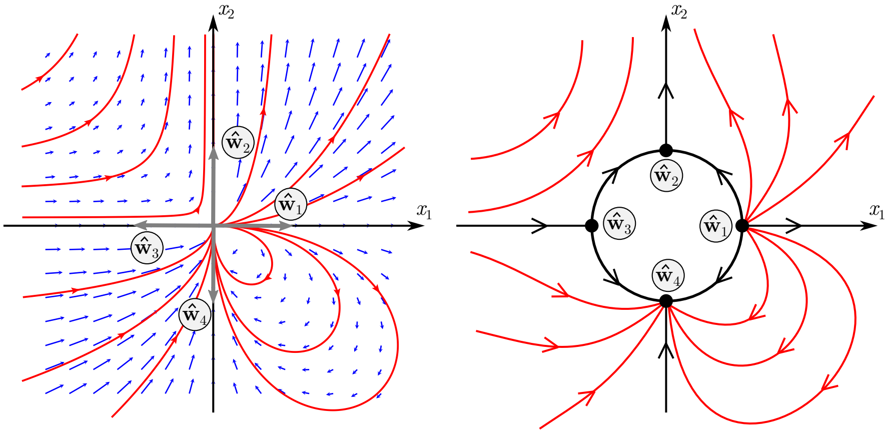

FIGURE 3. *Left panel: Phase space of the system* (3.10)–(3.11) *with four different types of limit directions. Right panel: illustration of the fast dynamics via a sketch of the phase space where the origin is visually blown up to a circle. Here limit directions are depicted by fixed points. The dominant limit directions* ($\hat{\mathbf{w}}_1, \hat{\mathbf{w}}_4$) *are connected to continuously many trajectories while each isolated limit direction* ($\hat{\mathbf{w}}_2, \hat{\mathbf{w}}_3$) *is connected to the single trivial trajectory.*

This categorization expresses whether a limit direction attracts the nearby trajectories *in the time direction of approaching the discontinuity set.* At a *dominant* limit direction, the trivial trajectory from Theorem 3.2 has a neighborhood where all trajectories are connected to Σ along the limit direction. At an *isolated* limit direction, there is a single isolated trajectory which is connected to Σ. At a *saddle-type* limit direction, there is a mixed behavior according to the stable and unstable directions of the saddle.

The types of limit directions in Definition 3.4 are visualized in Figure 3 showing the vector field of a codimension-2 example

$$\dot{x}_1 = w_1(w_1 + w_2 - w_2^2), \tag{3.10}$$

$$\dot{x}_2 = w_2(w_1 + w_2 + w_1^2), \tag{3.11}$$

where $w_1 = x_1/\sqrt{x_1^2 + x_2^2}$ and $w_2 = x_2/\sqrt{x_1^2 + x_2^2}$. The system leads to $R^\star = w_1 + w_2$ and $\mathbf{V}^\star = w_1 w_2(-w_2, w_1)$, and we obtain four limit directions: $\hat{\mathbf{w}}_1 = (1, 0)$ is repelling-dominant, $\hat{\mathbf{w}}_2 = (0, 1)$ is repelling-isolated, $\hat{\mathbf{w}}_3 = (-1, 0)$ is attracting-isolated, and $\hat{\mathbf{w}}_4 = (0, -1)$ is attracting-dominant.

When calculating the eigenvalues in Definition 3.4, the linearization of (2.25) at a fixed point $\hat{\mathbf{w}}$ can be written in the form

$$\mathbf{w}' = \mathbf{V}^\star_{\mathbf{w}}(\hat{\mathbf{w}}, \bar{\mathbf{x}}_t)(\mathbf{w} - \hat{\mathbf{w}}) + \mathcal{O}^2, \tag{3.12}$$

where $\mathcal{O}^2$ denote the higher-order terms, and the Jacobian $\mathbf{V}^\star_{\mathbf{w}}$ is calculated by

$$\mathbf{V}^\star_{\mathbf{w}} = \frac{\partial \mathbf{V}^\star}{\partial \mathbf{w}} - \frac{\partial \mathbf{V}^\star}{\partial \mathbf{w}} \mathbf{w}\mathbf{w}^\top. \tag{3.13}$$

The second term of (3.13) implements the projection onto the unit sphere $\mathbb{S}^{n-1}$: $\mathbf{w}^\top \mathbf{V}^\star_{\mathbf{w}} \mathbf{w} = 0$, that is, the radial dynamics is eliminated. Moreover, the dynamics along the sphere is preserved in (3.13), $\mathbf{V}^\star_\mathbf{w}\mathrm{d}\mathbf{w} = \partial\mathbf{V}^\star/\partial\mathbf{w}\,\mathrm{d}\mathbf{w}$, because all $\mathrm{d}\mathbf{w}$ from the tangent space of the sphere satisfy $\mathbf{w}^\top\mathrm{d}\mathbf{w} = 0$. Then, $\mathbf{V}^\star_\mathbf{w}$ is an $m \times m$ matrix with $m - n + 1$ trivial zero eigenvalues and $k \le n - 1$ nontrivial eigenvalues. In Definition 3.4, only these nontrivial eigenvalues $\lambda_1 \dots \lambda_k$ are considered, which corresponds to the dynamics on the unit sphere.

3.2.2. Limit cycles of w-limit cones of the system.

Definition 3.5. *Assume that $\mathbf{w}_c(\tau) : [0,T] \to \mathbb{R}^3$ is a limit cycle $\hat{\mathbf{w}}$ of the circumferential dynamics (2.25) with a time period T. Then, we call $\mathbf{w}_c$ a* limit cone *of the system (2.19) at $\bar{\mathbf{x}}$. Consider the average*

$$\overline{R^\star} = \frac{1}{T}\int_0^T R^\star(\mathbf{w}_c(\eta), \bar{\mathbf{x}}_t)\mathrm{d}\eta. \tag{3.14}$$

In the cases $\overline{R^\star} < 0$ or $\overline{R^\star} > 0$, $\mathbf{w}_c$ is called an attracting *or a* repelling *limit cone, respectively.*

By using the term limit *cone*, we identify the limit cycle $\mathbf{w}_c(\tau)$ and the cone $\mathcal{C} : \mathbb{R}^+ \times [0,T) \to \mathbb{R}^n$, $\mathcal{C}(\rho,\eta) = \bar{\mathbf{x}} + \rho\mathbf{w}_c(\eta)$. The concept of limit cones is illustrated by the right column of Figure 2.

Theorem 3.6. *Consider an attracting limit cone $\mathbf{w}_c$ at $\bar{\mathbf{x}} = (0, \mathbf{0}, \bar{\mathbf{x}}_t) \in \Sigma$. Then, there exists a trajectory $\mathbf{x}(t)$ of (2.19) and $\hat{t} \in \mathbb{R}$ such as*

$$\lim_{t \nearrow \hat{t}} \mathbf{x}(t) = \bar{\mathbf{x}} \tag{3.15}$$

and $\mathbf{x}(t)$ lies in the limit cone.

Proof. Consider a trajectory $\mathbf{x}(\tau) = (r(\tau)), \mathbf{w}(\tau), \mathbf{x}_t(\tau))$ with a starting point $r(0) = r_0 = \exp\rho_0$; $\mathbf{w}(0) = \mathbf{w}_0 = \mathbf{w}_c(\eta^*)$; $\mathbf{x}_t(0) = \mathbf{x}_{t,0}$ where $\eta^* \in [0, 2\pi]$. Equations (3.2) and (3.14) imply $\lim_{\tau\to\infty}\rho(\tau) = -\infty$, corresponding to $r \to 0$. The periodicity of $\mathbf{w}_c$ and (3.1) leads to $\rho(\tau + T) = \rho(\tau) + \overline{R^\star}T$. As the function $R^\star$ is bounded due to the properties of (2.3), the following values exist:

$$\Delta\rho_{\min} = \min_{\tau\in[0,T)}\left(\int_0^\tau R^\star(\mathbf{w}_c(\eta), \bar{\mathbf{x}}_t)\mathrm{d}\eta - \overline{R^\star}\tau\right), \tag{3.16}$$

$$\Delta\rho_{\max} = \max_{\tau\in[0,T)}\left(\int_0^\tau R^\star(\mathbf{w}_c(\eta), \bar{\mathbf{x}}_t)\mathrm{d}\eta - \overline{R^\star}\tau\right); \tag{3.17}$$

these are the extrema of the deviation of $\rho(\tau)$ from the approximate solution $\rho(\tau) \approx \rho_0 + \overline{R^\star}\tau$. Thus, we can make an estimation

$$\rho_0 + \overline{R^\star}\tau + \Delta\rho_{\min} \le \rho(\tau) \le \rho_0 + \overline{R^\star}\tau + \Delta\rho_{\max}. \tag{3.18}$$

Calculations analogous to (3.5) imply that on the original time scale, the time $\hat{t}$ required for reaching the discontinuity is finite, and it can be bounded by

$$\frac{-r_0\exp(\Delta\rho_{\min})}{\overline{R^\star}} \le \hat{t} \le \frac{-r_0\exp(\Delta\rho_{\max})}{\overline{R^\star}}. \tag{3.19}$$

Finally, by choosing the initial condition

$$\mathbf{x}_{t,0} = \bar{\mathbf{x}} - \int_0^{\hat{t}} \mathbf{F}_t^\star(\mathbf{w}(t), \bar{\mathbf{x}}_t)\mathrm{d}t, \tag{3.20}$$

the trajectory satisfies the statements of the theorem. ∎

In the theorem, a single trajectory from the starting point $\eta^* \in [0, 2\pi]$ was considered, but as η^* can be chosen from this interval, we get a continuous family of trajectories covering the limit cone and tending to $\bar{\mathbf{x}} \in \Sigma$. We can propose a similar theorem for the repelling case.

Theorem 3.7. *Consider a repelling limit cone $\mathbf{w}_c$ at $\bar{\mathbf{x}} = (0, \mathbf{0}, \bar{\mathbf{x}}_t) \in \Sigma$. Then, there exists a trajectory $\mathbf{x}(t)$ of (2.19) and $\hat{t} \in \mathbb{R}$ such as*

$$\lim_{t \searrow \hat{t}} \mathbf{x}(t) = \bar{\mathbf{x}} \tag{3.21}$$

and $\mathbf{x}(t)$ lies in the limit cone.

Proof. The proof is analogous to that of Theorem 3.6. ∎

Note that the case of limit cones is not relevant if $n = 1$, whereas for $n = 2$, at most one single limit cone can exist. This limit cone covers the full state space (the unit circle) of the fast dynamics. In this special case, the existence of trajectories with appropriate limits in the statements of Theorems 3.6–3.7 has been proved by [2] whereas the requirement of lying in the limit cone is trivially satisfied.

In the case of limit cones, a trajectory does not have a well-defined tangent when it approaches the discontinuity set. From this point of view, the surrounding trajectories in the fast subsystem are similar to the phase portrait of a focus point in a smooth system. But the convergence is, again, faster than exponential, and the oscillating solutions reach the discontinuity set in *finite time* either in forward or in backward direction of time. This point is illustrated by Example 4.4 and by Figure 6.

3.2.3. More complicated invariant sets of w. If a trajectory of the fast dynamics is not converging to a fixed point or periodic orbit, one needs to consider the infinite integral (3.2).

In some cases like convergence to a quasi-periodic orbit, the long-term average of $R^\star$ along trajectories is known to exist and converge to a well-defined limit value regardless of the exact initial conditions [36]. Hence

$$\overline{R^\star} = \lim_{\tau \to \pm\infty} \frac{\int_0^\tau R^\star(\mathbf{w}(\eta), \bar{\mathbf{x}}_t)d\eta}{\tau} \tag{3.22}$$

can be used in the analysis as done before. This case will not be elaborated further in this paper.

There are cases in which the analysis described above faces fundamental difficulties. In the case of trajectories converging to strange attractors, the limit (3.22) exists for almost all fixed initial conditions in the measure-theoretic sense; however, convergence is not robust in the topological sense: an arbitrarily small neighborhood of a typical initial condition contains possible initial conditions for which the value of $\overline{R^\star}$ is different by a finite amount or for which convergence does not occur at all [31]. It is certainly possible to prove the existence of trajectories starting or ending at the discontinuity manifold; nevertheless such a result has moderate practical significance. In the presence of any noise or uncertainty with respect to initial conditions, it may become unpredictable if a trajectory starts (ends) at the discontinuity or not.

For fast dynamics converging to a polycycle, a similar problem occurs. Even though the full system appears to have a “topological limit cone,” however, the radial dynamics along this manifold becomes ill-defined because the limit (3.22) usually fails to converge for most initial conditions [12]. Divergence is generated by the presence of multiple fixed points $\hat{\mathbf{w}}_j$ $j = 1, 2, \ldots, k$ along the polycycle. A trajectory starting at a general point of a polycycle will converge to one of these fixed points. For a trajectory converging to $\hat{\mathbf{w}}_j$, the limit (3.22) will be equal to the value $R^\star(\hat{\mathbf{w}}_j, \bar{\mathbf{x}}_t)$ corresponding to that fixed point. Other trajectories initiated in a small neighborhood of the polycycle do not converge to any of the individual points, but they asymptotically converge to the polycycle, such that they spend longer and longer times in small neighborhoods of the fixed points as they pass by. More detailed analysis [12] reveals that the time average of a scalar function like (3.22) along those trajectories oscillates in an interval (a, b) with $\min_j R^\star(\hat{\mathbf{w}}_j, \bar{\mathbf{x}}_t) < a < b < \max_j R^\star(\hat{\mathbf{w}}_j, \bar{\mathbf{x}}_t)$. It is possible that the interval (a, b) contains 0 in its interior. In such cases, r gets infinitely close to zero from time to time, but it diverges again and again. Hence there is no meaningful way to classify the radial dynamics as *attractive* or *repelling*. This behavior is illustrated by Example 4.5 below. Because the pathological behavior of radial dynamics and the lack of known applications where such limit sets may emerge, these cases are not examined further.

3.3. Limit directions and limit cones in the full system.

In the previous subsection, the multiple time scale analysis was applied to the approximate asymptotic system (2.24)–(2.26). In this subsection, we demonstrate that previous results related to fixed points and periodic orbits of the fast dynamics can be applied to the full system (2.21)–(2.23) as well. Because of the difficulties associated with all other types of attractors (see Section 3.2.3) those cases are not investigated in the rest of the paper.

The set $r = 0$ is an invariant set of (2.21)–(2.23) where the dynamics is determined by

$$r' = 0, \tag{3.23}$$

$$\mathbf{w}' = \mathbf{V}^\star(\mathbf{w}, \mathbf{x}_t), \tag{3.24}$$

$$\mathbf{x}_t' = 0. \tag{3.25}$$

As $\mathbf{x}_t' = 0$, the set $r = 0$ can be partitioned to invariant subsets (*layers*) parametrized by $\mathbf{x}_t$. For a chosen layer $\mathbf{x}_t = \bar{\mathbf{x}}_t$, (3.24) coincides with the fast dynamics (2.25) of the asymptotic approximate system. Thus, (3.24) can be considered as a vector field depending smoothly on the parameter $\mathbf{x}_t$. Consequently, in the case of a *hyperbolic* fixed point or limit cycle of (3.24), the local dynamics of the system is topologically equivalent in all layers in the neighborhood of $\mathbf{x}_t = \bar{\mathbf{x}}_t$.

In the local neighborhood of $r = 0$ and $\mathbf{x}_t = \bar{\mathbf{x}}_t$, the vector fields can be written into Taylor series form

$$R(r,\mathbf{w},\mathbf{x}_t) = R^\star(\mathbf{w},\bar{\mathbf{x}}_t) + R^\star_r(\mathbf{w},\bar{\mathbf{x}}_t)r + R^\star_{\mathbf{x}_t}(\mathbf{w},\bar{\mathbf{x}}_t)(\mathbf{x}_t-\bar{\mathbf{x}}_t) + \mathcal{O}^2, \tag{3.26}$$

$$\mathbf{V}(r,\mathbf{w},\mathbf{x}_t) = \mathbf{V}^\star(\mathbf{w},\bar{\mathbf{x}}_t) + \mathbf{V}^\star_r(\mathbf{w},\bar{\mathbf{x}}_t)r + \mathbf{V}^\star_{\mathbf{x}_t}(\mathbf{w},\bar{\mathbf{x}}_t)(\mathbf{x}_t-\bar{\mathbf{x}}_t) + \mathcal{O}^2, \tag{3.27}$$

$$\mathbf{F}_t(r,\mathbf{w},\mathbf{x}_t) = \mathbf{F}^\star_t(\mathbf{w},\bar{\mathbf{x}}_t) + \mathbf{F}^\star_{t,r}(\mathbf{w},\bar{\mathbf{x}}_t)r + \mathbf{F}^\star_{t,\mathbf{x}_t}(\mathbf{w},\bar{\mathbf{x}}_t)(\mathbf{x}_t-\bar{\mathbf{x}}_t)+\mathcal{O}^2, \tag{3.28}$$

where the meaning of the subscripts is

$$R^*_r(\mathbf{w},\bar{\mathbf{x}}_t) = \left.\frac{\partial R(r,\mathbf{w},\mathbf{x}_t)}{\partial r}\right|_{r=0,\mathbf{x}_t=\bar{\mathbf{x}}_t}, \tag{3.29}$$

$$R^*_{\mathbf{x}_t}(\mathbf{w},\bar{\mathbf{x}}_t) = \left.\frac{\partial R(r,\mathbf{w},\mathbf{x}_t)}{\partial \mathbf{x}_t}\right|_{r=0,\mathbf{x}_t=\bar{\mathbf{x}}_t}, \tag{3.30}$$

and $\mathcal{O}^2$ denotes the higher-order terms. Then, the dynamics (2.21)–(2.23) becomes

$$r' = rR^\star(\mathbf{w},\bar{\mathbf{x}}_t) + \mathcal{O}^2, \tag{3.31}$$

$$\mathbf{w}' = \mathbf{V}^\star(\mathbf{w},\bar{\mathbf{x}}_t) + \mathbf{V}^\star_r(\mathbf{w},\bar{\mathbf{x}}_t)r + \mathbf{V}^\star_{\mathbf{x}_t}(\mathbf{w},\bar{\mathbf{x}}_t)(\mathbf{x}_t-\bar{\mathbf{x}}_t) + \mathcal{O}^2, \tag{3.32}$$

$$\mathbf{x}'_t = r\mathbf{F}^\star_t(\mathbf{w},\bar{\mathbf{x}}_t) + \mathcal{O}^2. \tag{3.33}$$

In what follows we shall discuss limit directions and limit cones separately with similar conclusions in the two cases.

3.3.1. Limit directions. Consider a fixed point $\hat{\mathbf{w}}$ with $\mathbf{V}^\star(\hat{\mathbf{w}},\bar{\mathbf{x}}_t) = \mathbf{0}$. Then, from (3.12) and (3.31)–(3.33), the full linearized system at the fixed point $(r,\mathbf{w},\mathbf{x}_t) \equiv (0,\hat{\mathbf{w}},\bar{\mathbf{x}}_t)$ is

$$\begin{pmatrix} r' \\ \tilde{\mathbf{w}}' \\ \tilde{\mathbf{x}}'_t \end{pmatrix} = \begin{pmatrix} R^\star(\hat{\mathbf{w}},\bar{\mathbf{x}}_t) & 0 & 0 \\ \mathbf{V}^\star_r(\hat{\mathbf{w}},\bar{\mathbf{x}}_t) & \mathbf{V}^\star_{\mathbf{w}}(\hat{\mathbf{w}},\bar{\mathbf{x}}_t) & \mathbf{V}^\star_{\mathbf{x}_t}(\hat{\mathbf{w}},\bar{\mathbf{x}}_t) \\ \mathbf{F}^\star_t(\hat{\mathbf{w}},\bar{\mathbf{x}}_t) & \mathbf{0} & \mathbf{0} \end{pmatrix} \begin{pmatrix} r \\ \tilde{\mathbf{w}} \\ \tilde{\mathbf{x}}_t \end{pmatrix} + \mathcal{O}^2, \tag{3.34}$$

where $\tilde{\mathbf{w}} = \mathbf{w} - \hat{\mathbf{w}}$, $\tilde{\mathbf{x}}_t = \mathbf{x}_t - \bar{\mathbf{x}}_t$, and $\mathbf{V}^\star_{\mathbf{w}}$ was defined in (3.13). The characteristic equation of the matrix in (3.34) is

$$(R^\star(\hat{\mathbf{w}},\bar{\mathbf{x}}_t) - \lambda)\cdot \det\left(\mathbf{V}^\star_{\mathbf{w}}(\hat{\mathbf{w}},\bar{\mathbf{x}}_t) - \lambda\mathbf{I}^n\right)\cdot \det\left(-\lambda\mathbf{I}^{m-n}\right) = 0, \tag{3.35}$$

where $\mathbf{I}^n$ denotes the $n \times n$ identity matrix. Then, we have the following three types of eigenvalues and eigenvectors of the linearized system:

1. The roots of $\det\left(\mathbf{V}^\star_{\mathbf{w}}(\hat{\mathbf{w}},\bar{\mathbf{x}}_t) - \lambda\mathbf{I}^n\right) = 0$ are the eigenvalues of $\mathbf{V}^\star_{\mathbf{w}}(\hat{\mathbf{w}},\bar{\mathbf{x}}_t)$. As it was explained at (3.12), there are $k \le n-1$ nontrivial eigenvalues and a trivial zero eigenvalue. It can be shown that the corresponding eigenvectors of (3.34) have the form $\mathbf{v} = (0,\mathbf{v}_{\mathbf{w}},\mathbf{0})$ where $\mathbf{v}_{\mathbf{w}}$ coincide with the eigenvectors of the fast subsystem (3.12).
2. The roots of $\det\left(-\lambda\mathbf{I}^{m-n}\right) = 0$ are $m-n$ zero eigenvalues. The corresponding eigenvectors have the form $\mathbf{v} = (0,\mathbf{v}_{\mathbf{w}},\mathbf{v}_{\mathbf{x}_t})$ and they can be calculated by solving

   $$\mathbf{V}^\star_{\mathbf{w}}(\hat{\mathbf{w}},\bar{\mathbf{x}}_t)\mathbf{v}_{\mathbf{w}} + \mathbf{V}^\star_{\mathbf{x}_t}(\hat{\mathbf{w}},\bar{\mathbf{x}}_t)\mathbf{v}_{\mathbf{x}_t} = 0. \tag{3.36}$$

   The expression (3.36) is strongly related to the total derivative of the right-hand side of the fast dynamics (3.24) at a fixed point. In fact, (3.36) determines the tangent space of a *critical manifold* (see [22, p. 12]) determined by $\mathbf{V}^\star(\mathbf{w},\mathbf{x}_t) = \mathbf{0}$, which contains the fixed points in the different layers of the fast dynamics.

3. At the eigenvalue $R^\star(\hat{\mathbf{w}},\bar{\mathbf{x}}_t)$, regularity conditions should be checked. In the singular cases when either $\mathbf{V}^\star_{\mathbf{w}}(\hat{\mathbf{w}},\bar{\mathbf{x}}_t) - R^\star(\hat{\mathbf{w}},\bar{\mathbf{x}}_t)\mathbf{I}^n$ is a singular matrix or $R^\star(\hat{\mathbf{w}},\bar{\mathbf{x}}_t)=0$, the corresponding eigenvector coincides with that of the two previous types of eigenvalues. In the regular case when $R^\star(\hat{\mathbf{w}},\bar{\mathbf{x}}_t)$ is neither zero nor an eigenvalue of $\mathbf{V}^\star_{\mathbf{w}}(\hat{\mathbf{w}},\bar{\mathbf{x}}_t)$, the corresponding eigenvector has the form $\mathbf{v}=(1,\mathbf{v}_{\mathbf{w}},\mathbf{v}_{\mathbf{x}_t})$ satisfying

$$\begin{pmatrix} \mathbf{V}^\star_{\mathbf{w}}(\hat{\mathbf{w}},\bar{\mathbf{x}}_t) - R^\star(\hat{\mathbf{w}},\bar{\mathbf{x}}_t)\mathbf{I}^n & \mathbf{V}^\star_{\mathbf{x}_t}(\hat{\mathbf{w}},\bar{\mathbf{x}}_t) \\ \mathbf{0} & -R^\star(\hat{\mathbf{w}},\bar{\mathbf{x}}_t)\mathbf{I}^{m-n} \end{pmatrix} \begin{pmatrix} \mathbf{v}_{\mathbf{w}} \\ \mathbf{v}_{\mathbf{x}_t} \end{pmatrix} = \begin{pmatrix} \mathbf{V}^\star_r(\hat{\mathbf{w}},\bar{\mathbf{x}}_t) \\ \mathbf{F}^\star_t(\hat{\mathbf{w}},\bar{\mathbf{x}}_t) \end{pmatrix}. \tag{3.37}$$

The first two types of eigenvectors do not have a component in the r direction, so they are not related to trajectories leaving or arriving at the discontinuity at $r=0$. The only eigenvector transversal to $r=0$ is the eigenvector of $R^\star(\hat{\mathbf{w}},\bar{\mathbf{x}}_t)$ in the regular case. One side of the eigenvector points to $r<0$, which is irrelevant in our original system. However, at $r>0$, this eigenvector corresponds to a stable ($R^\star(\hat{\mathbf{w}},\bar{\mathbf{x}}_t)<0$) or unstable ($R^\star(\hat{\mathbf{w}},\bar{\mathbf{x}}_t)>0$) manifold where trajectories from $r>0$ are connected to the selected point $\bar{\mathbf{x}}\in\Sigma$. This is the same behavior that was proposed in Theorems 3.2 and 3.3 in the case of *attracting* and *repelling* limit directions, respectively. Moreover, as the eigenvalues of $\mathbf{V}^\star_{\mathbf{w}}(\hat{\mathbf{w}},\bar{\mathbf{x}}_t)$ appear both in (3.12) and in (3.34), the *dominant*, *saddle-type*, and *isolated* properties from Definition 3.4 are inherited to the full system in the case of *hyperbolic* fixed points of the fast dynamics.

Hence, we conclude that in the nonsingular cases, the multiple time scale analysis of limit directions of the asymptotic approximate system (2.24)–(2.26) can be used for the qualitative analysis of the full system (2.21)–(2.23).

3.3.2. Limit cones.

Consider now a periodic orbit $\hat{\mathbf{w}}(\tau)$ of (3.24) with period T such that $\hat{\mathbf{w}}'=\mathbf{V}^\star(\hat{\mathbf{w}},\bar{\mathbf{x}}_t)$ (where dependence of $\hat{\mathbf{w}}$ on τ has been hidden). The full linearized system at the periodic orbit $(r,\mathbf{w},\mathbf{x}_t)\equiv(0,\hat{\mathbf{w}}(\tau),\bar{\mathbf{x}}_t)$ is again given by (3.34) with the only difference being that the coefficient matrix is now time-dependent and periodic.

The linear stability of periodic solutions of (3.34) is analyzed via a linearized Poincaré map. In particular, consider a Poincaré section $\mathcal{P}$ transversal to the flow through the point $(r,\mathbf{w},\mathbf{x}_t)\equiv(0,\hat{\mathbf{w}}(0),\bar{\mathbf{x}}_t)$. This point is a fixed point of the Poincaré map. The linearized Poincaré map is determined by (3.34) and takes the form

$$\begin{pmatrix} r(\tilde{T}) \\ \tilde{\mathbf{w}}(\tilde{T}) \\ \tilde{\mathbf{x}}_t(\tilde{T}) \end{pmatrix} = \mathbf{P}\begin{pmatrix} r(0) \\ \tilde{\mathbf{w}}(0) \\ \tilde{\mathbf{x}}_t(0) \end{pmatrix} + \mathcal{O}^2, \tag{3.38}$$

where $\tilde{T}$ is the time of first return to the Poincaré section. Note that $\tilde{T}\neq T$ in general; however, for $r(0)=\tilde{\mathbf{w}}(0)=\tilde{\mathbf{x}}_t(0)=0$, we have $\tilde{T}=T$.

In general, there is no simple formula to express $\mathbf{P}$ in terms of the equation of the linearized flow; however, the special structure of the coefficient matrix in (3.34) allows us to express $\mathbf{P}$ as follows.

Notice first that the linearized dynamics of r is given by (3.34) as $r'=R^\star(\hat{\mathbf{w}},\bar{\mathbf{x}}_t)r$. This homogeneous, linear, nonautonomous scalar equation yields

$$r(\tau) = r(0)e^{\int_0^\tau R^\star(\hat{\mathbf{w}}(\xi),\bar{\mathbf{x}}_t)d\xi}. \tag{3.39}$$

Second, the linearized dynamics of $\tilde{\mathbf{x}}_t$ is given by (3.34) as $\tilde{\mathbf{x}}_t' = F_t^\star(\hat{\mathbf{w}}, \bar{\mathbf{x}}_t)r$. Using (3.39), we can now express

$$\tilde{\mathbf{x}}_t(\tau) = \tilde{\mathbf{x}}_t(0) + r(0)\int_0^\tau F_t^\star(\hat{\mathbf{w}}(\zeta), \bar{\mathbf{x}}_t)e^{\int_0^\zeta R^\star(\hat{\mathbf{w}}(\xi),\bar{\mathbf{x}}_t)d\xi}d\zeta. \tag{3.40}$$

In a last step, we find $\tilde{\mathbf{w}}(\tau)$ from the remaining set of equations given by (3.34):

$$\tilde{\mathbf{w}}' = \mathbf{V}_r^\star(\hat{\mathbf{w}}, \bar{\mathbf{x}}_t)r + \mathbf{V}_{\mathbf{w}}^\star(\hat{\mathbf{w}}, \bar{\mathbf{x}}_t)\tilde{\mathbf{w}} + \mathbf{V}_{\mathbf{x}_t}^\star(\hat{\mathbf{w}}, \bar{\mathbf{x}}_t)\tilde{\mathbf{x}}_t + \mathcal{O}^2 \tag{3.41}$$

which is a nonautonomous, periodic, linear, inhomogenous vector-valued ODE. The solution of that system is

$$\begin{aligned}\tilde{\mathbf{w}}(\tau) &= \boldsymbol{\Phi}(\tau)\tilde{\mathbf{w}}(0)\ldots\\ &+\int_0^t \boldsymbol{\Phi}(\tau)\boldsymbol{\Phi}^{-1}(\xi)\left(\mathbf{V}_r^\star(\hat{\mathbf{w}}(\xi), \bar{\mathbf{x}}_t)r(\xi) + \mathbf{V}_{\mathbf{x}_t}^\star(\hat{\mathbf{w}}(\xi), \bar{\mathbf{x}}_t)\tilde{\mathbf{x}}_t(\xi)\right)d\xi,\end{aligned} \tag{3.42}$$

where $\boldsymbol{\Phi}(\tau)$ is the so-called principal matrix solution of the equation (see Theorem 1.2.5 in [9]). We will not need the exact form of $\boldsymbol{\Phi}$. Note that the first term in (3.42) is the solution of the homogeneous part of the equation, which is identical to the asymptotic fast dynamics (2.25).

According to (3.39), (3.40), $r(\tau), \tilde{\mathbf{x}}_t(\tau)$ are linear functions of $r(0)$ and $\tilde{\mathbf{x}}_t(0)$, and thus we can write the Poincaré map as

$$\begin{aligned}\begin{pmatrix} r(\tilde{T}) \\ \tilde{\mathbf{w}}(\tilde{T}) \\ \tilde{\mathbf{x}}_t(\tilde{T})\end{pmatrix} &= \begin{pmatrix} r(T) \\ \tilde{\mathbf{w}}(T) \\ \tilde{\mathbf{x}}_t(T)\end{pmatrix} + \mathcal{O}^2\\ &= \begin{pmatrix} e^{\int_0^T R^\star(\hat{\mathbf{w}}(\xi),\bar{\mathbf{x}}_t)d\xi} & 0 & 0 \\ * & \boldsymbol{\Phi}(T) & ** \\ *** & \mathbf{0} & \mathbf{I}^{m-n}\end{pmatrix}\begin{pmatrix} r(0) \\ \tilde{\mathbf{w}}(0) \\ \tilde{\mathbf{x}}_t(0)\end{pmatrix} + \mathcal{O}^2.\end{aligned} \tag{3.43}$$

The star symbols in the matrix represent closed-form expressions, which are omitted for brevity. It is notable that the matrix in (3.43) has a similar structure to the matrix in (3.34). The characteristic equation of the matrix in (3.43) is

$$\left(e^{\int_0^T R^\star(\hat{\mathbf{w}}(\xi),\bar{\mathbf{x}}_t)d\xi} - \lambda\right)\cdot\det\left(\boldsymbol{\Phi}(T) - \lambda\mathbf{I}^n\right)\cdot\det\left(\mathbf{I}^{m-n} - \lambda\mathbf{I}^{m-n}\right) = 0, \tag{3.44}$$

which allows us to draw conclusions similar to the case of limit directions. In particular,

1. the roots of $\det\left(\boldsymbol{\Phi}(T) - \lambda\mathbf{I}^n\right) = 0$ are the eigenvalues determining the linear stability of the periodic solution of the asymptotic fast dynamics (2.25);
2. the roots of $\det\left(\mathbf{I}^{m-n} - \lambda\mathbf{I}^{m-n}\right)$ are $m-n$ unit eigenvalues;
3. the eigenvalue $e^{\int_0^T R^\star(\hat{\mathbf{w}}(\xi),\bar{\mathbf{x}}_t)d\xi}$ exceeds 1 (corresponding to instability) if $\bar{R}^* > 0$ (see (3.14)) and it is below 1 (corresponding to stability) in the opposite case. The case of $\bar{R}^* = 0$ is degenerate and out of scope of this work.

As before, the eigenvectors corresponding to the first two types of eigenvalues have no radial components whereas the eigenvector of the last eigenvalues does have such a component. Again, we find that the *attracting/repelling* and *dominant/saddle-type/isolated* properties of the full system are inherited by the asymptotic approximate system.

4. Examples.

We now present several simple examples to cover all the important cases detected in the analysis above and to illustrate the behavior of these systems. In Examples 4.1 to 4.3, the limit sets of the fast dynamics are fixed points; the purpose of these examples is to illustrate how the limit directions organize the dynamics in the neighborhood of the discontinuity set. Example 4.4 exemplifies local dynamics in the presence of a limit cone. Finally, Example 4.5 illustrates pathologic behavior if the fast dynamics converges to a polycycle. In Examples 4.6 to 4.8, simple mechanical examples are shown demonstrating codimension-1, 2 and 3 discontinuities. In these examples, we focus on the radial and circumferential dynamics, and thus the tangential dynamics is either trivial or missing. The tangential dynamics is analyzed in detail in section 5.

4.1. Fast dynamics converging to fixed points.

Example 4.1 (isolated limit directions). Consider the system

$$\mathbf{F}(\mathbf{x}) = \begin{pmatrix} 2x_1/\sqrt{x_1^2+x_2^2+x_3^2} \\ x_2/\sqrt{x_1^2+x_2^2+x_3^2} \\ -x_3//\sqrt{x_1^2+x_2^2+x_3^2} \\ 1 \end{pmatrix}, \tag{4.1}$$

where $\mathbf{x} \in \mathbb{R}^4$. (In the long formulae, we denote the vectors by columns matrices.) In this case, $\mathbf{x}_o = (x_1, x_2, x_3, 0)$, $\mathbf{x}_t = (0, 0, 0, x_4)$ and the codimension-3 discontinuity surface Σ is defined by $x_1 = x_2 = x_3 = 0$. Polar decomposition yields

$$R(r, \mathbf{w}, \mathbf{x}_t) = 2w_1^2 + w_2^2 - w_3^2, \tag{4.2}$$

$$\mathbf{V}(r, \mathbf{w}, \mathbf{x}_t) = (2w_1, w_2, -w_3, 0) - (2w_1^2 + w_2^2 - w_3^2)(w_1, w_2, w_3, 0), \tag{4.3}$$

$$\mathbf{F}_t(\mathbf{w}, \mathbf{x}_t) = (0, 0, 0, 1), \tag{4.4}$$

where

$$r = \sqrt{x_1^2+x_2^2+x_3^2}, \tag{4.5}$$

$$\mathbf{w} = (x_1, x_2, x_3, 0)/\sqrt{x_1^2+x_2^2+x_3^2} = (w_1, w_2, w_3, 0). \tag{4.6}$$

In this case, none of the functions above depends on r or x_4, hence $R \equiv R^\star$, $\mathbf{V} \equiv \mathbf{V}^\star$, and $\mathbf{F}_t \equiv \mathbf{F}_t^\star$ (see (2.13)–(2.15)). The tangential dynamics in the x_4 direction is now trivial.

The fast dynamics $\dot{\mathbf{w}} = \mathbf{V}^\star(\mathbf{w}, \mathbf{x}_t)$ has six invariant points denoted by $\hat{\mathbf{w}}_1 \dots \hat{\mathbf{w}}_6$, each corresponding to a limit direction of the system (Figure 4(a)). From Definition 3.1, the sign of $R^\star(\mathbf{w}, \mathbf{x}_t)$ decides whether the limit direction is attracting or repelling. From the eigenvalues of the fixed point (see (3.12)), Definition 3.4 can be used to determine the dominant or isolated property of the limit direction.

The properties of the limit directions of the system are summarized in Table 1. We can see that for this simple example, the limit directions appear in pairs, $\hat{\mathbf{w}}_1 = -\hat{\mathbf{w}}_2$, $\hat{\mathbf{w}}_3 = -\hat{\mathbf{w}}_4$, $\hat{\mathbf{w}}_5 = -\hat{\mathbf{w}}_6$, and the properties of the two limit directions in each pair are identical. Generic trajectories of the fast (circumferential) dynamics of the system start from $\hat{\mathbf{w}}_5$ or $\hat{\mathbf{w}}_6$ and end at $\hat{\mathbf{w}}_1$ or $\hat{\mathbf{w}}_2$, and the unit sphere is partitioned by the stable manifolds of the saddles

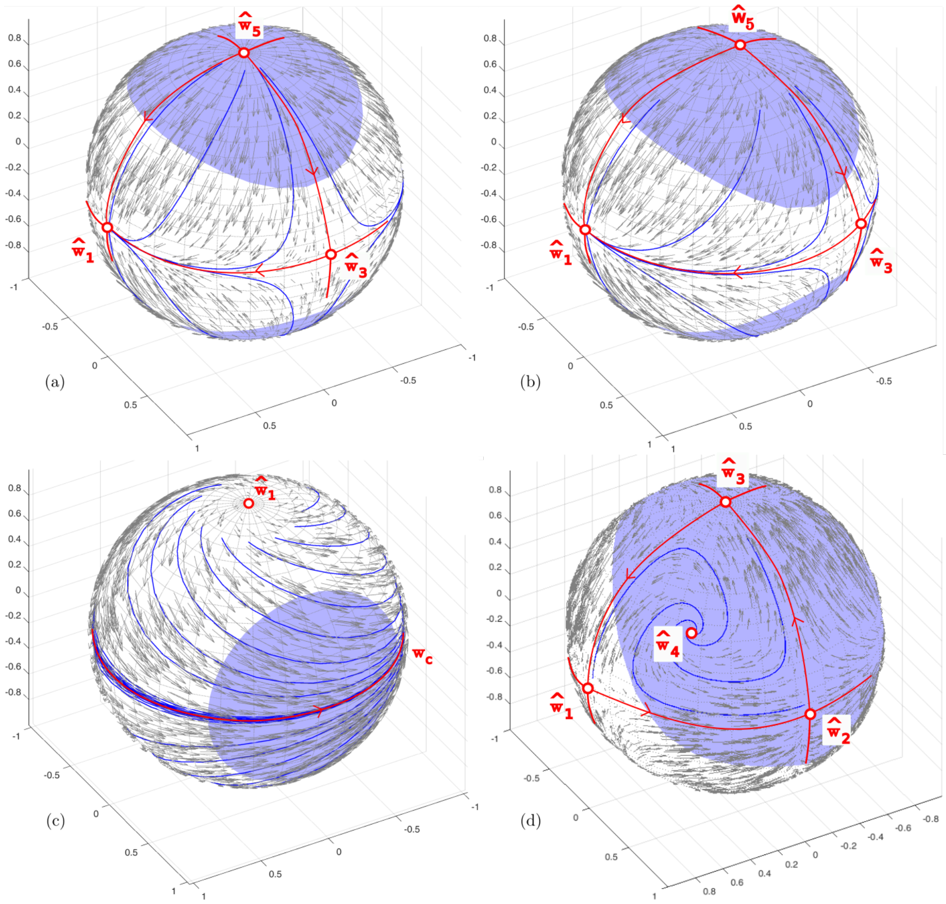

FIGURE 4. *Illustration of the limit vector fields for* (a) *Example 4.1,* (b) *Example 4.3,* (c) *Example 4.4, and* (d) *Example 4.5. Thin curves (blue online) denote some trajectories, thick curves (red online) depict* (a), (b), (d) *heteroclinic orbits and* (c) *periodic orbit of the circumferential dynamics. Fixed points are denoted by circles. Dark shading denotes those directions where $R^\star < 0$, i.e., trajectories move toward the discontinuity in the radial direction. Note that the limit vector field of Example 4.2 is identical to* (a) *except that the shading is inverted.*

TABLE 1
Limit directions of (4.1) *in Example* 4.1.

	Location	$R^\star(\hat{\mathbf{w}}, \bar{\mathbf{x}})$	Fixed point	Limit direction
$\hat{\mathbf{w}}_1$	$(1, 0, 0, 0)$	2	stable node	repelling-isolated
$\hat{\mathbf{w}}_2$	$(-1, 0, 0, 0)$	2	stable node	repelling-isolated
$\hat{\mathbf{w}}_3$	$(0, 1, 0, 0)$	1	saddle	repelling-saddle
$\hat{\mathbf{w}}_4$	$(0, -1, 0, 0)$	1	saddle	repelling-saddle
$\hat{\mathbf{w}}_5$	$(0, 0, 1, 0)$	-1	unstable node	attracting-isolated
$\hat{\mathbf{w}}_6$	$(0, 0, -1, 0)$	-1	unstable node	attracting-isolated

$\hat{\mathbf{w}}_3$ and $\hat{\mathbf{w}}_4$. The signs of $R^\star$ at the fixed points reveal that all nodes are *isolated*, hence generic trajectories do not reach the discontinuity. In forward time, the trajectories diverge radially along the repelling directions $\hat{\mathbf{w}}_1$ or $\hat{\mathbf{w}}_2$, and in backward time, they diverge along the attracting directions $\hat{\mathbf{w}}_5$ or $\hat{\mathbf{w}}_6$ as illustrated by numerical simulation in Figure 5(a). There are only special trajectories which are connected to the discontinuity either forward or backward in time.

The analysis of the limit directions outlined above makes it possible to categorize the trajectories in the vicinity of a point $\bar{\mathbf{x}}$ of the discontinuity set Σ. We can find

- generic trajectories which are not connected to Σ,
- two isolated trajectories ending at Σ along $\hat{\mathbf{w}}_5$ and $\hat{\mathbf{w}}_6$,
- two isolated trajectories starting from Σ along $\hat{\mathbf{w}}_1$ and $\hat{\mathbf{w}}_2$,
- trajectories in the unstable manifolds of $\hat{\mathbf{w}}_3$ and $\hat{\mathbf{w}}_4$ starting from Σ along $\hat{\mathbf{w}}_3$ and $\hat{\mathbf{w}}_4$. (These trajectories correspond to heteroclinic orbits of the fast dynamics in the plane $x_3 = 0$.)

Example 4.2 (dominant limit directions). Consider a variant of the previous example where $\mathbf{V}^\star(\mathbf{w}, \mathbf{x}_t)$ is kept the same and $R^\star(\mathbf{w}, \mathbf{x}_t)$ is multiplied by -1. For that, consider the system

$$\mathbf{F}(\mathbf{x}) = \mathbf{F}^1(\mathbf{x}) - 2\mathbf{w}^\top \mathbf{F}^1(\mathbf{x})\mathbf{w}, \tag{4.7}$$

where $\mathbf{w} = 1/\sqrt{x_1^2 + x_2^2 + x_3^2} \cdot (x_1, x_2, x_3, 0)$ and $\mathbf{F}^1(\mathbf{x})$ equals to the vector field (4.1) of the previous example. Then, we get

$$R^\star(\mathbf{w}, \bar{\mathbf{x}}_t) = -2w_1^2 - w_2^2 + w_3^2, \tag{4.8}$$

$$\mathbf{V}^\star(\mathbf{w}, \bar{\mathbf{x}}_t) = (2w_1, w_2, -w_3, 0) - (2w_1^2 + w_2^2 - w_3^2)(w_1, w_2, w_3, 0), \tag{4.9}$$

$$\mathbf{F}_t^\star(\mathbf{w}, \bar{\mathbf{x}}_t) = (0, 0, 0, 1). \tag{4.10}$$

Calculations similar to the previous example yield the results summarized in Table 2. The main difference between Examples 1 and 2 is that now all nodes are *dominant*. That is, the typical trajectories in the vicinity of the discontinuity set are connected to Σ (Figure 5(b)). We can identify the following types of trajectories:

- generic trajectories starting from Σ along $\hat{\mathbf{w}}_5$ or $\hat{\mathbf{w}}_6$ and ending at Σ along $\hat{\mathbf{w}}_1$ or $\hat{\mathbf{w}}_2$,
- trajectories in the unstable manifolds of $\hat{\mathbf{w}}_3$ and $\hat{\mathbf{w}}_4$ starting from Σ along $\hat{\mathbf{w}}_3$ and $\hat{\mathbf{w}}_4$,
- two isolated trajectories starting from Σ along $\hat{\mathbf{w}}_5$ or $\hat{\mathbf{w}}_6$ and leaving the vicinity of Σ,
- four isolated incoming trajectories ending at Σ along $\hat{\mathbf{w}}_1$, $\hat{\mathbf{w}}_2$, $\hat{\mathbf{w}}_3$, and $\hat{\mathbf{w}}_4$.

Example 4.3 (nontrivial limit directions). In order to reduce the complexity of calculations, Examples 4.1 to 4.2 contain such symmetries that the limit directions are organized into pairs opposite to each other and having the same properties. This symmetry can be broken by adding a constant term to (4.1). Consider the system

$$\mathbf{F}(\mathbf{x}) = \begin{pmatrix} 2x_1/\sqrt{x_1^2 + x_2^2 + x_3^2} + 1/2 \\ x_2/\sqrt{x_1^2 + x_2^2 + x_3^2} \\ -x_3//\sqrt{x_1^2 + x_2^2 + x_3^2} \\ 1 \end{pmatrix}. \tag{4.11}$$

By following the calculation steps of Example 4.1, one obtains the results summarized in Table 3. The number and type of limit directions in Examples 4.1 and 4.3 are the same.

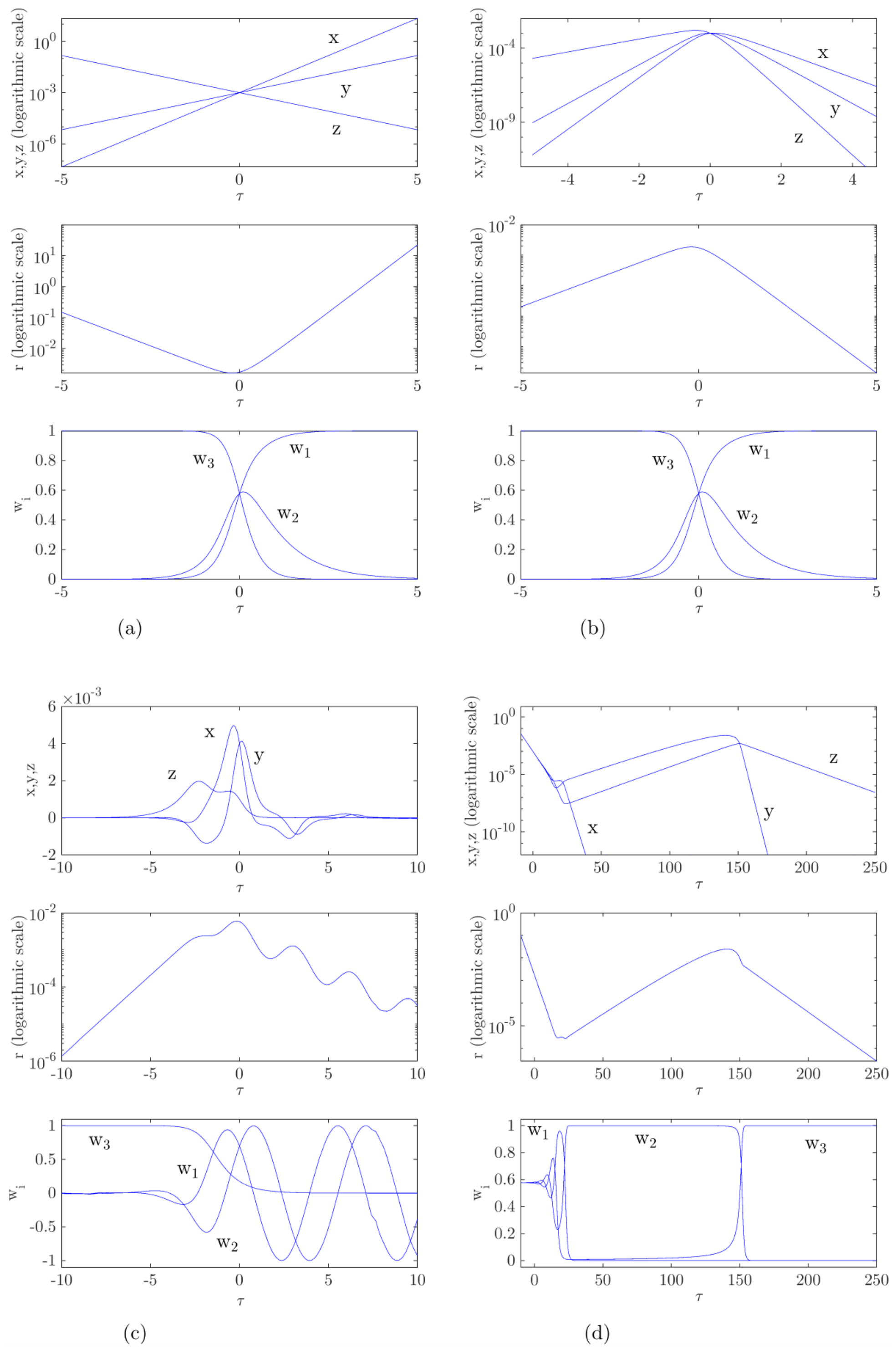

FIGURE 5. *Numerically determined trajectories of* (a) *Example* 4.1, (b) *Example* 4.2, (c) *Example* 4.4, *and* (d) *Example* 4.5. *Initial conditions at* $t = 0$ *are* (a), (b) $x = y = z = 10^{-3}$, (c) $x = y = 4 \cdot 10^{-3}$, $z = 10^{-3}$, *and* (d) $x = y = 10^{-3}$, $z = 1.013 \cdot 10^{-3}$. *Each trajectory was followed forward and backward in time.*

TABLE 2
Limit directions of (4.7) in Example 4.2.

	Location	$R^\star(\hat{\mathbf{w}}, \bar{\mathbf{x}})$	Fixed point	Limit direction
$\hat{\mathbf{w}}_1$	$(1,0,0,0)$	-2	stable node	attracting-dominant
$\hat{\mathbf{w}}_2$	$(-1,0,0,0)$	-2	stable node	attracting-dominant
$\hat{\mathbf{w}}_3$	$(0,1,0,0)$	-1	saddle	attracting-saddle
$\hat{\mathbf{w}}_4$	$(0,-1,0,0)$	-1	saddle	attracting-saddle
$\hat{\mathbf{w}}_5$	$(0,0,1,0)$	1	unstable node	repelling-dominant
$\hat{\mathbf{w}}_6$	$(0,0,-1,0)$	1	unstable node	repelling-dominant

TABLE 3
Limit directions of (4.11) in Example 4.3.

	Location	$R^\star(\hat{\mathbf{w}}, \bar{\mathbf{x}})$	Fixed point	Limit direction
$\hat{\mathbf{w}}_1$	$(1,0,0,0)$	$5/2$	stable node	repelling-isolated
$\hat{\mathbf{w}}_2$	$(-1,0,0,0)$	$3/2$	stable node	repelling-isolated
$\hat{\mathbf{w}}_3$	$(-\frac{1}{2}, \frac{\sqrt{3}}{2}, 0, 0)$	1	saddle	repelling-saddle
$\hat{\mathbf{w}}_4$	$(-\frac{1}{2}, -\frac{\sqrt{3}}{2}, 0, 0)$	1	saddle	repelling-saddle
$\hat{\mathbf{w}}_5$	$(-\frac{1}{6}, 0, \frac{\sqrt{35}}{6}, 0)$	-1	unstable node	attracting-isolated
$\hat{\mathbf{w}}_6$	$(-\frac{1}{6}, 0, -\frac{\sqrt{35}}{6}, 0)$	-1	unstable node	attracting-isolated

Thus, the local dynamics is topologically equivalent (see Figure 4(b)). However, the geometry of the phase space has changed: the symmetries mentioned above are broken, and the limit directions are not constrained to trivial pairs any more.

4.2. Fast dynamics converging to a limit cycle.

Example 4.4. Consider the system

$$\mathbf{F}(\mathbf{x}) = \begin{pmatrix} -x_2/\sqrt{x_1^2+x_2^2+x_3^2} \\ x_1/\sqrt{x_1^2+x_2^2+x_3^2} \\ -x_3/\sqrt{x_1^2+x_2^2+x_3^2} \\ 1 \end{pmatrix} + \left(\frac{3x_1^2+4x_3^2}{x_1^2+x_2^2+x_3^2} - 2 \right) \cdot \mathbf{w}, \tag{4.12}$$

where $\mathbf{w} = 1/\sqrt{x_1^2+x_2^2+x_3^2} \cdot (x_1, x_2, x_3, 0)$. The polar transformation now reveals

$$R^\star(\mathbf{w}, \bar{\mathbf{x}}) = 3w_1^2 + 3w_3^2 - 2, \tag{4.13}$$

$$\mathbf{V}^\star(\mathbf{w}, \bar{\mathbf{x}}) = (-w_2 + w_1 w_3^2, w_1 + w_2 w_3^2, -w_3 + w_3^3, 0), \tag{4.14}$$

$$\mathbf{F}_t^\star(\mathbf{w}, \bar{\mathbf{x}}) = (0,0,0,1). \tag{4.15}$$

Inspection of the third component of $\mathbf{V}$ reveals that the sets $w_3 = 0$ and $w_3 = \pm 1$ are invariant. The first one corresponds to a circle $\mathbf{w}_c$, and the second one corresponds to two fixed points $\hat{\mathbf{w}}_1 = (0,0,1,0)$ and $\hat{\mathbf{w}}_2 = (0,0,-1,0)$. Considering the fast dynamics of $\mathbf{w}$, the generic trajectories start from $\hat{\mathbf{w}}_1$ or $\hat{\mathbf{w}}_2$ and converge to the limit cycle $\mathbf{w}_c$ (Figure 4(c)). The dynamics of w_1, w_2 over $\mathbf{w}_c$ is given by

$$w_1' = -w_2, \tag{4.16}$$

$$w_2' = w_1, \tag{4.17}$$

which generates periodic motion.

Consider now the radial dynamics (Figure 4(c)). From (4.13), we get $R^\star = 1$ for both fixed points $\hat{\mathbf{w}}_1$ and $\hat{\mathbf{w}}_2$; thus, the two related limit directions are *repelling-dominant* type. The radial dynamics at $\mathbf{w}_c$ is determined by the time average (3.14). By introducing the polar angle ϕ with $w_1 = \cos\phi$, $w_2 = \sin\phi$, the periodic motion corresponds to $\phi = \phi_0 + \tau$ and (3.14) is equivalent to

$$\overline{R^\star} = \int_0^{2\pi} 3w_1^2 - 2\,\mathrm{d}\phi = \int_0^{2\pi} 3\cos^2\phi - 2\,\mathrm{d}\phi = -\pi. \tag{4.18}$$

That is, the limit cone is *attracting-dominant*. Consequently, the possible types of nearby trajectories are

- generic trajectories starting from Σ along the limit directions $\hat{\mathbf{w}}_1$ or $\hat{\mathbf{w}}_2$ and ending in Σ along the limit cone $\mathbf{w}_c$ (see Figure 5(b));
- two isolated trajectories starting from Σ along $\hat{\mathbf{w}}_1$ or $\hat{\mathbf{w}}_2$ and leaving the vicinity of Σ;
- a continuous family of incoming trajectories ending at Σ along $\mathbf{w}_c$.

It is straightforward to show that the plane $x_3 = 0$ is an invariant plane of the full system (4.12) with the dynamics

$$\dot{x}_1 = -w_2 + w_1(3w_1^2 - 2), \tag{4.19}$$

$$\dot{x}_2 = w_1 + w_2(3w_1^2 - 2), \tag{4.20}$$

where $w_1 = w_1/\sqrt{x_1^2 + x_2^2}$ and $w_2 = w_2/\sqrt{x_1^2 + x_2^2}$. We know from (3.19) that the trajectories in the vicinity of a limit cone converge in finite time. This is confirmed by the numerical simulation of (4.19)–(4.20), which can be seen in Figure 6.

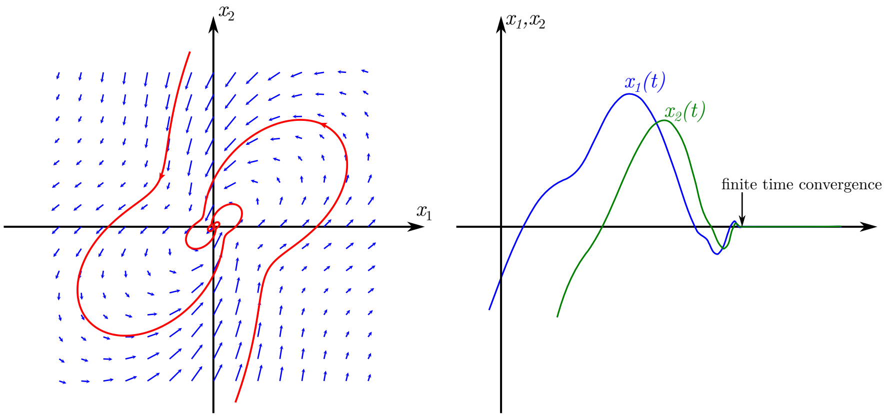

FIGURE 6. *Oscillatory behavior related to a limit cone in Example 4.4. Left panel: in the invariant plane $x_3 = 0$, the system exhibits oscillations with a decay faster than exponential. Right panel: the trajectories converge to the origin in finite time.*

4.3. Fast dynamics converging to a polycycle.

Example 4.5. Consider the system

$$\mathbf{F}(\mathbf{x}) = \begin{pmatrix} \frac{x_1(x_1-x_2-x_3)-x_1x_2}{x_1^2+x_2^2+x_3^2} \\ \frac{x_2(x_1-x_2-x_3)-x_2x_3}{x_1^2+x_2^2+x_3^2} \\ \frac{x_3(x_1-x_2-x_3)-x_3x_1}{x_1^2+x_2^2+x_3^2} \\ 1 \end{pmatrix}. \tag{4.21}$$

The polar transformation results in

$$R^\star(\mathbf{w}, \bar{\mathbf{x}}_t) = w_1 - w_2 - w_3 - w_1^2 w_2 - w_2^2 w_3 - w_3^2 w_1, \tag{4.22}$$

$$\mathbf{V}^\star(\mathbf{w}, \bar{\mathbf{x}}_t) = \begin{pmatrix} -w_1w_2 + w_1^3 w_2 + w_1 w_2^2 w_3 + w_1^2 w_3^2 \\ -w_2w_3 + w_2^3 w_3 + w_2 w_3^2 w_1 + w_2^2 w_1^2 \\ -w_3w_1 + w_3^3 w_1 + w_3 w_1^2 w_2 + w_3^2 w_2^2 \\ 1 \end{pmatrix}, \tag{4.23}$$

$$\mathbf{F}_t^\star(\mathbf{w}, \bar{\mathbf{x}}_t) = (0,0,0,1). \tag{4.24}$$

We will focus on the circumferential dynamics in the *positive octant of the state space*, that is, $0 \le w_1, w_2, w_3 \le 1$ (Figure 4(d)). Here, the existence of four fixed points can be verified by substitution into (4.23): $\hat{\mathbf{w}}_1 = (1,0,0,0)$, $\hat{\mathbf{w}}_2 = (0,1,0,0)$, $\hat{\mathbf{w}}_3 = (0,0,1,0)$, $\hat{\mathbf{w}}_4 = 1/\sqrt{3} \cdot (1,1,1,0)$.

If $w_3 = 0$, then the dynamics becomes

$$\mathbf{V}(r, \mathbf{w}, \mathbf{x}_t) = \left(-w_1w_2, w_2^2 w_1^2, 0, 1\right), \tag{4.25}$$

that is, in the selected octant, $w_1' < 0 < w_2'$ and $w_3' = 0$. Hence there is a heteroclinic orbit from $\hat{\mathbf{w}}_1$ to $\hat{\mathbf{w}}_2$. Similar heteroclinic orbits exist from $\hat{\mathbf{w}}_2$ to $\hat{\mathbf{w}}_3$ and from $\hat{\mathbf{w}}_3$ to $\hat{\mathbf{w}}_1$.

In order to uncover the full phase portrait of the circumferential dynamics, we consider a Lyapunov-like function $L(\mathbf{w}) = \ln w_1 + \ln w_2 + \ln w_3$. It is straightforward to prove by using (2.6) and the inequality of arithmetic and geometric means that $L(\mathbf{w})$ attains its maximum value over the positive octant of the unit sphere at $\hat{\mathbf{w}}_4$. Furthermore, it does not have any local extrema, and it diverges to minus infinity as one approaches any of the previously found heteroclinic orbits due to $\lim_{x \searrow 0} \ln x = -\infty$. The directional time derivative of L along $\mathbf{w}(t)$ is given by

$$\begin{aligned} \frac{d}{d\tau} L(\mathbf{w}(t)) &= \sum_{i=1}^{3} \partial L / \partial w_i w_i' = \sum_{i=1}^{3} w_i^{-1} V_i \\ &= -w_1 - w_2 - w_3 + w_1^2(w_2+w_3) + w_2^2(w_3+w_1) \\ &\quad + w_3^2(w_1+w_2) + w_1^2 w_2 + w_2^2 w_3 + w_3^2 w_1. \end{aligned} \tag{4.26}$$

The rearrangement inequality [15] and (2.6) imply

$$\begin{aligned} \frac{d}{d\tau} L(\mathbf{w}(t)) &\le -w_1 - w_2 - w_3 + w_1^2(w_2+w_3)) + w_2^2(w_3+w_1) \\ &\quad + w_3^2(w_1+w_2) + w_1^3 + w_2^3 + w_3^3 \\ &= -w_1 - w_2 - w_3 + (w_1^2+w_2^2+w_3^2)(w_1+w_2+w_3) = 0. \end{aligned} \tag{4.27}$$

Hence, L is monotonically decreasing along trajectories, which means that general trajectories converge to $\hat{\mathbf{w}}_4$ backward in time and to the $\hat{\mathbf{w}}_1 \to \hat{\mathbf{w}}_2 \to \hat{\mathbf{w}}_3 \to \hat{\mathbf{w}}_1$ polycycle forward in time. Convergence to a polycycle means that trajectories visit close neighborhoods of $\hat{\mathbf{w}}_1, \hat{\mathbf{w}}_2, \hat{\mathbf{w}}_3$ in alternating order and spend longer and longer time before transition to the next point. The rapidly increasing amount of time spent in close neighborhoods of the invariant points is responsible for the divergent behavior of the time average (3.22) as pointed out in section 3.2.3.

It can be shown from (4.22) that $R^\star(\hat{\mathbf{w}}, \bar{\mathbf{x}})$ takes the values $1, -1, -1, -2/\sqrt{3}$ at the fixed points $\hat{\mathbf{w}}_1, \hat{\mathbf{w}}_3, \hat{\mathbf{w}}_3, \hat{\mathbf{w}}_4$, respectively (Figure 4(d)). That is, trajectories converging to the polycycle visit both repelling ($\hat{\mathbf{w}}_1$) and attracting ($\hat{\mathbf{w}}_2, \hat{\mathbf{w}}_3$) fixed points. More detailed analysis following [12] also reveals that the time average (3.22) oscillates in an interval (a, b) with $-1 < a < 0 < b < 1$. Accordingly, r gets infinitely close to zero from time to time, but it diverges again and again as illustrated by our numerical simulation in Figure 5(d).

4.4. Application to motion under dry friction.

The equations of motion of rigid bodies under dry friction provide natural examples of dynamical systems with discontinuity sets. Below we present three simple examples, all demonstrated on a slipping block: Example 4.6 shows the classical textbook example of Filippov systems, Example 4.7 contains a codimension-2 discontinuity, and Example 4.8 demonstrates codimension-3 discontinuity.

Example 4.6 (slip motion in one dimension). Consider the motion of a block slipping on a horizontal line in one dimension (see Figure 7(a)). The velocity of the block is denoted by u, and we push the block by a constant force $P \geq 0$. By assuming that the block is *slipping* on the plane in the presence of Coulomb friction, the dynamics is described by a single differential equation

$$m\dot{u} = P - \mu m g \frac{u}{|u|}, \tag{4.28}$$

where m is the mass of the block, g denotes the gravitational acceleration, and μ is the friction coefficient between the block and the plane. The single point $u = 0$ is a trivial codimension-1 discontinuity set. The decomposition of variables yields $\mathbf{x}_o = (u)$, $r = |u|$, $\mathbf{w} = (w_1)$, $w_1 = u/|u|$. As the codimension of the discontinuity set is 1, the circumferential dynamics is trivial, $\mathbf{V}^\star = 0$, and the limit of the radial dynamics becomes $R^\star(\mathbf{w}) = Pw_1/m - \mu g$. The two trivial limit directions are $\hat{\mathbf{w}}_1 = (-1)$ and $\hat{\mathbf{w}}_2 = (1)$, related to the slipping of the block to left and the right, respectively. The direction $\hat{\mathbf{w}}_1$ is always attracting; $\hat{\mathbf{w}}_2$ is attracting for $P < \mu m g$ and repelling for $P < \mu m g$.

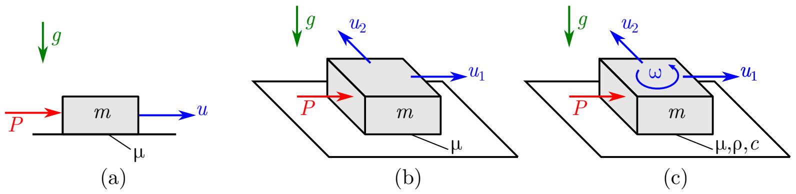

FIGURE 7. *Three examples of discontinuous dynamics induced by dry friction: a block slipping in one dimension (panel* (a)*) and in two dimensions (panel* (b)*) under the effect of Coulomb friction, and a block slipping in two dimensions under the effect of Coulomb friction combined with spinning friction (panel* (c)*).*

The results of the analysis are consistent with the well-known behavior of this trivial mechanical system:

- For a small pushing force ($P < \mu mg$), the *sticking* of the block ($u = 0$) is realizable, because small perturbations of the *slipping* velocity u are eliminated by the system in finite time, and the block starts sticking, again.
- For a higher pushing force ($P > \mu mg$), sticking is not realizable: The limit direction $\hat{\mathbf{w}}_2$ becomes repelling, which makes the block slip to the right immediately. But if the perturbation causes slipping to the left ($u < 0$), a sticking phase occurs for a moment before permanent slipping to the right.

Example 4.7 (slip motion in two dimensions). Consider a block similar to the previous example, which moves freely on a plane in two dimensions (with the forces being three-dimensional). Let u_1 and u_2 denote the components of the slipping velocity and let the pushing force $P > 0$ be parallel to u_1 (see Figure 7(b)). Then, by assuming Coulomb friction, the dynamics in the state space (u_1, u_2) is given by the system

$$m\dot{u}_1 = P - \mu mg \frac{u_1}{\sqrt{u_1^2 + u_2^2}}, \qquad m\dot{u}_2 = -\mu mg \frac{u_2}{\sqrt{u_1^2 + u_2^2}}. \tag{4.29}$$

The state space has a codimension-2 discontinuity set $u_1 = u_2 = 0$. Decomposition of the variables yields $\mathbf{x}_o = (u_1, u_2)$, $r = \sqrt{u_1^2 + u_2^2}$, and $\mathbf{w} = (w_1, w_2)$ where $w_1 = u_1/\sqrt{u_1^2 + u_2^2}$ and $w_2 = u_2/\sqrt{u_1^2 + u_2^2}$. The limit values at the discontinuity are $R^\star(\mathbf{w}) = Pw_1/m - \mu g$, and $\mathbf{V}^\star(\mathbf{w}) = P/m \cdot (w_2^2, -w_1 w_2)$. By solving $\mathbf{V}^\star(\mathbf{w}) = \mathbf{0}$, one obtains the limit directions $\hat{\mathbf{w}}_1 = (-1, 0)$, $\hat{\mathbf{w}}_2 = (1, 0)$, which are physically the same as in the previous example. By direct calculation, it can be shown that $\hat{\mathbf{w}}_1$ is attracting-isolated, whereas $\hat{\mathbf{w}}_2$ is attracting-dominant for $P < \mu mg$ and repelling-isolated for $P > \mu mg$.

The mechanical consequences are the following:

- The condition $P < \mu mg$ of the realizable slipping motion is the same as that in the planar model. The effect of a small perturbation in the slipping velocities disappears in finite time. Moreover, the slipping velocity vanishes typically along the *dominant* limit direction $\hat{\mathbf{w}}_2$, that is, the velocity is opposite to the pushing force just before sticking initiates.
- In the case $P > \mu mg$, there is a repelling and an attracting limit direction, both of which are *isolated*. That is, the generic behavior of the adjacent trajectories is avoiding the discontinuity at $u_1 = u_2 = 0$. Accordingly, small perturbations typically initiate slip motion in the direction of the pushing force without creating an instantaneous sticking state.

Example 4.8 (slip motion under drilling torque). If the friction force is modeled as a distributed force field over a finite contact area, the resultant force and torque need to be considered at the same time (see Figure 7(c)). Based on the results of [23] and [21], the combined effect of the slipping velocities u_1 and u_2 and the *spinning* angular velocity ω can be described by a simple phenomenological model leading to the equations

$$m\dot{u}_1 = P - \frac{\mu mg u_1}{\sqrt{u_1^2 + u_2^2 + \rho^2\omega^2}}, \tag{4.30}$$

$$m\dot{u}_2 = -\frac{\mu m g u_2}{\sqrt{u_1^2 + u_2^2 + \rho^2\omega^2}}, \tag{4.31}$$

$$J\dot{\omega} = -\frac{c\mu J g \omega}{\sqrt{u_1^2 + u_2^2 + \rho^2\omega^2}}. \tag{4.32}$$

In (4.30)–(4.32), ρ is a parameter with dimension length, which is related to the size of the contact area between the block and the plane. J is the moment of inertia of the block, and c is a dimensionless parameter assumed to be in the range $0 < c < 1$. Based on the phase space $\mathbf{x}_o = (u_1, u_2, \rho\omega)$, the calculations presented above lead to the following results:

- For $(1 - c)\mu m g < P < \mu m g$, there is an attracting-isolated limit direction $\hat{\mathbf{w}}_1 = (-1, 0, 0)$ and an attracting-dominant limit direction $\hat{\mathbf{w}}_2 = (1, 0, 0)$. For $\mu m g < P$, $\hat{\mathbf{w}}_2$ becomes repelling-isolated. In these two cases, the block behaves similarly to the previous model.
- For $P < (1 - c)\mu m g$, $\hat{\mathbf{w}}_2 = (1, 0, 0)$ becomes *attracting-saddle* type, and two further limit directions $\hat{\mathbf{w}}_{3,4} = (\cos\delta, 0, \pm\sin\delta)$ appear with

  $$\delta = \arccos(P/(\mu m g(1 - c))), \tag{4.33}$$

  which are both attracting-*dominant*. In this new scenario, the sticking state is typically reached along these new directions where the u_1 component of the slipping velocity and the spinning angular velocity ω are related by $u_1 \sin\delta \pm \rho\omega\cos\delta = 0$.

Note that in the case $c > 1$ the analysis can be done analogously. The value of the parameter c depends on the geometry and the pressure distribution of the contact area, which are not discussed here.

5. Sliding and crossing.

In the previous section, we determined and analyzed the possible trajectories which tend to the discontinuity set Σ in positive or negative direction of time. Now, our goal is to explore the possibilities to concatenate these trajectories and to extend the dynamics to Σ. This goal resulted in the concept of *sliding* and *crossing* in piecewise smooth dynamical systems.

It was mentioned in subsection 2.2 that in addition to the vector field outside Σ, we need further information at discontinuity to determine this concatenation and the sliding and crossing regions. In the case of piecewise smooth systems, the jump at the discontinuity can be expressed by using switching variables (containing the nonsmooth terms). The choice of this expression modifies significantly the sliding and crossing behavior, which can be analyzed in detail by exploring the *hidden dynamics* inside the discontinuity set blown up to a boundary layer; see, for example, [17]. The simplest choice to connect the vector field through the discontinuity set is Filippov's convex method.

The main focus of the present paper has been on the structure of the vector field and trajectories in the vicinity of the discontinuity set. Nevertheless, in this section, we make initial steps toward defining sliding and crossing at the discontinuity set. The analysis is restricted to the convex method. In this case, the *sliding dynamics* can be obtained by linear expressions, which is shown for the codimension-1 case in [7, p. 76], and for the codimension-2 case in [2]. Now, we extend these concepts to the general codimension-n case. The analysis of nonlinear sliding [35, 6, 29, 17] is left for future work.

5.1. Crossing and sliding regions. We have seen that the circumferential dynamics $\mathbf{V}^\star(\mathbf{w}, \bar{\mathbf{x}}_t)$ may have several types of invariant sets (see subsection 3.1). We now restrict the analysis to systems where the invariant sets are fixed points (related to attracting and repelling limit directions) and limit cycles (related to attracting and repelling limit cones). The points $\bar{\mathbf{x}}_t \in \Sigma$ can be categorized according to the attracting or repelling property of these objects.

Definition 5.1 (crossing and sliding). *Consider a point $\mathbf{x} = \bar{\mathbf{x}}_t \in \Sigma$ and assume that all the invariant sets of $\mathbf{V}^\star(\mathbf{w}, \bar{\mathbf{x}}_t)$ are fixed points and limit cycles.*

- *We call $\bar{\mathbf{x}}_t$ a* crossing *point of Σ if there is at least one attracting limit direction or limit cone and there is at least one repelling limit direction or limit cone.*
- *We call $\bar{\mathbf{x}}_t$ an* attracting sliding *point of Σ if all the limit directions and limit cones are attracting.*
- *We call $\bar{\mathbf{x}}_t$ a* repelling sliding *point of Σ if all the limit directions and limit cones are repelling.*

Note that alternatively, repelling sliding could be called "escaping," and then attracting sliding could be referred to simply as "sliding." Both naming conventions are used in relation to classical Filippov systems.

According to Definition 5.1, the discontinuity set Σ is partitioned to the *crossing region* Σ_c, the *attracting sliding region* Σ_a, and the *repelling sliding region* Σ_r. The special cases at the boundaries between these regions are not analyzed here.

At a *crossing* point, there exist at least one trajectory of $\mathbf{F}$ ending at $\bar{\mathbf{x}}_t$ and at least one trajectory starting from $\bar{\mathbf{x}}_t$, which trajectories can be connected through the discontinuity. However, unlike in classical Filippov systems, there are typically *several* starting and ending trajectories at $\bar{\mathbf{x}}_t$ and the actual connection of them is ambiguous. This problem could possibly be resolved by regularization as done at the singularities of Filippov systems [20], but it is beyond the scope of the paper. Now, we can say that this definition of crossing gives the *possibility* to concatenate the trajectories at the current point of the discontinuity set.

At a *sliding* point, connecting trajectories through the discontinuity is clearly not possible because either all the trajectories end at $\bar{\mathbf{x}}_t$ (attracting sliding) or they all start from $\bar{\mathbf{x}}_t$ (repelling sliding). That is, the trajectories are "stuck" into the discontinuity set in forward or backward direction of time. In order to achieve a complete description of the behavior of the system, we define the *sliding dynamics* inside Σ in the following.

5.2. Sliding dynamics. At the sliding region, the straightforward way to complete the dynamics is to create a *sliding vector field* $\tilde{\mathbf{F}} : \Sigma_a \cup \Sigma_r \to \mathbb{R}^m$. At a point $\bar{\mathbf{x}}_t \in \Sigma$, the sliding vector $\tilde{\mathbf{F}}(\bar{\mathbf{x}}_t)$ is assumed to be generated by the limit vector field $\mathbf{F}^*(\mathbf{w}, \bar{\mathbf{x}}_t)$, which dependence can be either *convex* or *nonconvex*. Already in the codimension-1 discontinuity of the classical Filippov system, the nonconvex combination introduces an additional level of complexity and several new phenomena (see [17] for an overview). Now, the analysis is restricted to the sliding vector field from *convex combination.*

5.2.1. Definition of sliding dynamics.

Definition 5.2 (sliding vector from convex combination). *Consider a point $\bar{\mathbf{x}}_t \in \Sigma$. The vector $\tilde{\mathbf{F}}(\bar{\mathbf{x}}_t)$ is called a (convex)* sliding vector *if there exists a function $\alpha : \mathbb{S}^{n-1} \to [0, 1]$ satisfying*

$$\int_{\mathbb{S}^{n-1}} \alpha(\mathbf{w})\mathrm{d}\mathbf{w} = 1, \tag{5.1}$$

$$\int_{\mathbb{S}^{n-1}} \alpha(\mathbf{w}) \cdot \mathbf{F}_o^\star(\mathbf{w}, \bar{\mathbf{x}}_t)\mathrm{d}\mathbf{w} = \mathbf{0}, \tag{5.2}$$

$$\int_{\mathbb{S}^{n-1}} \alpha(\mathbf{w}) \cdot \mathbf{F}_t^\star(\mathbf{w}, \bar{\mathbf{x}}_t)\mathrm{d}\mathbf{w} = \tilde{\mathbf{F}}(\bar{\mathbf{x}}_t). \tag{5.3}$$

That is, the resulting vector $\tilde{\mathbf{F}}(\bar{\mathbf{x}}_t)$ is tangent to Σ, and the orthogonal component $\mathbf{F}_o =$ vanishes. We assume that in the codimension-1 case, the integration in (5.1)–(5.2) reduces to the summation of the two elements in $\mathbb{S}^0$. With this construction, two fundamental questions arise:

- Does the sliding vector $\tilde{\mathbf{F}}(\bar{\mathbf{x}}_t)$ *exist* for any point $\bar{\mathbf{x}}_t$ in the sliding region $\Sigma_a \cup \Sigma_r$? In the codimension-1 case of Filippov systems, $\bar{\mathbf{x}}_t$ being in the closure of the sliding region is *equivalent* to the existence of $\tilde{\mathbf{F}}(\bar{\mathbf{x}}_t)$ ([7, p. 76]). In the codimension-2 case of extended Filippov systems, $\bar{\mathbf{x}}_t$ being in the sliding region is a *sufficient but not necessary* condition of the existence of $\tilde{\mathbf{F}}(\bar{\mathbf{x}}_t)$ [2]. We expect that this is the case also in the higher codimension cases, but we do not prove this.
- Is this construction $\tilde{\mathbf{F}}(\bar{\mathbf{x}}_t)$ *unique*? In the codimension-1 case, the convex sliding vector is unique; however, nonuniqueness arises at the intersection of discontinuity sets [8, 16, 19]. In the codimension-2 case, the sliding vector is *nonunique* except for a restricted class of systems, which satisfy certain linearity conditions [2]. As we point out below, the same thing happens in the higher codimensional case: (5.1)–(5.3) generate a *convex hull* of the set $\mathbf{F}^\star(\mathbb{S}^{n-1}, \bar{\mathbf{x}}_t)$, and the intersection of this set with Σ is typically not a single point. We do not attempt to resolve nonuniqueness in general; however, we identify an important class of systems where the sliding vector is unique.

In those systems where the existence and uniqueness of the sliding vector are ensured, we can create the system

$$\dot{\mathbf{x}} = \tilde{\mathbf{F}}(\mathbf{x}) \tag{5.4}$$

in $\mathbf{x} \in \Sigma_a \cup \Sigma_c$ which we call the *sliding dynamics*. The sliding dynamics is a consistent complement of the original nonsmooth system (2.1) in the sliding region.

5.2.2. Systems with unique sliding vector. We now establish a subclass of the systems where the sliding vector field is unique. The case described in the next theorem is practically important because mechanical problems with dry friction often have this form of equation.

Theorem 5.3. *Consider a point $\bar{\mathbf{x}}_t \in \Sigma$. Assume that the limit vector field* (2.19) *has the form*

$$\mathbf{F}_o^\star(\mathbf{w}, \bar{\mathbf{x}}_t) = \begin{pmatrix} \mathbf{A}_o(\bar{\mathbf{x}}_t) \\ \mathbf{0} \end{pmatrix} \cdot \mathbf{b}(\mathbf{w}, \bar{\mathbf{x}}_t) + \begin{pmatrix} \mathbf{c}_o(\bar{\mathbf{x}}_t) \\ \mathbf{0} \end{pmatrix}, \tag{5.5}$$

$$\mathbf{F}_t^\star(\mathbf{w}, \bar{\mathbf{x}}_t) = \begin{pmatrix} \mathbf{0} \\ \mathbf{A}_t(\bar{\mathbf{x}}_t) \end{pmatrix} \cdot \mathbf{b}(\mathbf{w}, \bar{\mathbf{x}}_t) + \begin{pmatrix} \mathbf{0} \\ \mathbf{c}_t(\bar{\mathbf{x}}_t) \end{pmatrix}, \tag{5.6}$$

where $\mathbf{b}, \mathbf{c}_o \in \mathbb{R}^n$, $\mathbf{c}_t \in \mathbb{R}^{m-n}$, $\mathbf{A}_o \in \mathbb{R}^{n\times n}$ is an invertible matrix, and $\mathbf{A}_t \in \mathbb{R}^{n\times(m-n)}$. Assume that a sliding vector $\tilde{\mathbf{F}}(\bar{\mathbf{x}}_t)$ satisfying (5.1)–(5.3) *exists. Then, the sliding vector is unique and it is determined by*

$$\tilde{\mathbf{F}}(\bar{\mathbf{x}}_t) = \begin{pmatrix} \mathbf{0} \\ \mathbf{c}_t(\bar{\mathbf{x}}_t) - \mathbf{A}_t(\bar{\mathbf{x}}_t)\mathbf{A}_o^{-1}(\bar{\mathbf{x}}_t)\mathbf{c}_o(\bar{\mathbf{x}}_t) \end{pmatrix}. \tag{5.7}$$

Proof. The formulation (5.5)–(5.6) ensures that for fixed $\bar{\mathbf{x}}_t$, the values of $\mathbf{F}^\star$ for any $\mathbf{w}$ belong to an n-plane $\mathbf{F} \in \mathbb{R}^m$ described in a parametric form. By eliminating $\mathbf{b}(\mathbf{w}, \bar{\mathbf{x}}_t)$, (5.5)–(5.6) can be rearranged to the explicit form

$$\mathbf{F}_t^\star(\mathbf{w}, \bar{\mathbf{x}}_t) = \begin{pmatrix} \mathbf{0} \\ \tilde{\mathbf{A}}(\bar{\mathbf{x}}_t) \end{pmatrix} \mathbf{F}_o^\star(\mathbf{w}, \bar{\mathbf{x}}_t) + \begin{pmatrix} \mathbf{0} \\ \tilde{\mathbf{c}}(\bar{\mathbf{x}}_t) \end{pmatrix}, \tag{5.8}$$

where

$$\tilde{\mathbf{A}}(\bar{\mathbf{x}}_t) = \mathbf{A}_t(\bar{\mathbf{x}}_t)\mathbf{A}_o^{-1}(\bar{\mathbf{x}}_t), \qquad \tilde{\mathbf{c}}(\bar{\mathbf{x}}_t) = \mathbf{c}_t(\bar{\mathbf{x}}_t) - \mathbf{A}_t(\bar{\mathbf{x}}_t)\mathbf{A}_o^{-1}(\bar{\mathbf{x}}_t)\mathbf{c}_o(\bar{\mathbf{x}}_t). \tag{5.9}$$

By using (5.8), we can transform (5.3) into

$$\tilde{\mathbf{F}}(\bar{\mathbf{x}}_t) = \begin{pmatrix} \mathbf{0} \\ \tilde{\mathbf{A}}(\bar{\mathbf{x}}_t) \end{pmatrix} \int_{\mathbb{S}^{n-1}} \alpha(\mathbf{w}) \cdot \mathbf{F}_o^\star(\mathbf{w}, \bar{\mathbf{x}}_t) \mathrm{d}\mathbf{w} + \begin{pmatrix} \mathbf{0} \\ \tilde{\mathbf{c}}(\bar{\mathbf{x}}_t) \end{pmatrix} \int_{\mathbb{S}^{n-1}} \alpha(\mathbf{w}) \mathrm{d}\mathbf{w}. \tag{5.10}$$

Then, further substitution of (5.1) and (5.2) into (5.10) yields (5.7). ∎

In summary, if we are able to put the vector field into the form (5.5)–(5.6), then not only is the uniqueness of the sliding vector field ensured but we have an explicit formula (5.7). Many mechanical problems with dry friction induce dynamics that satisfies (5.5)–(5.6) with $\mathbf{b}(\mathbf{w}, \bar{\mathbf{x}}_t) = \mathbf{w}$. However, the presented theorem applies to a more general class of systems.

5.3. Sliding dynamics in mechanical problems with dry friction.

Example 5.4 **(rolling-slipping ball).** The examples in section 4 contained a trivial dynamics of the tangential variables $\mathbf{x}_t$, and thus, the concept of sliding and crossing were not demonstrated. In the last example, we show a simple mechanical model which exhibits crossing and sliding regions, and where the sliding dynamics describes the mechanical effect of rolling.

Consider a homogeneous ball undergoing a combination of roll and slip motion on a plane in the presence of a viscous medium (see Figure 8(a)). The radius of the ball is ρ, its mass is m, and its moment of inertia is $2/5 \cdot m\rho^2$. The friction coefficient at the contact point is μ, and the *effective* gravitational acceleration is denoted by g (buoyancy is included). The state of the ball is described by the variables $\mathbf{x} = (u_1, u_2, v_1, v_2)$ where u_1, u_2 are the velocity components of the contact point and v_1, v_2 are the velocity components of the center of gravity of the ball. The effect of the medium is modeled simply as a linear drag force at the center of gravity of the ball with components $-Kv_1$ and $-Kv_2$ where K is a drag parameter. Then, the Euler–Lagrange equations of the ball lead to the differential equation

$$\begin{pmatrix} \dot{u}_1 \\ \dot{u}_2 \\ \dot{v}_1 \\ \dot{v}_2 \end{pmatrix} = \mathbf{F}(\mathbf{x}) = \begin{pmatrix} -\frac{7}{2}\mu g \frac{u_1}{\sqrt{u_1^2+u_2^2}} - \frac{K}{m} v_1 \\ -\frac{7}{2}\mu g \frac{u_2}{\sqrt{u_1^2+u_2^2}} - \frac{K}{m} v_2 \\ -\mu g \frac{u_1}{\sqrt{u_1^2+u_2^2}} - \frac{K}{m} v_1 \\ -\mu g \frac{u_2}{\sqrt{u_1^2+u_2^2}} - \frac{K}{m} v_2 \end{pmatrix}. \tag{5.11}$$

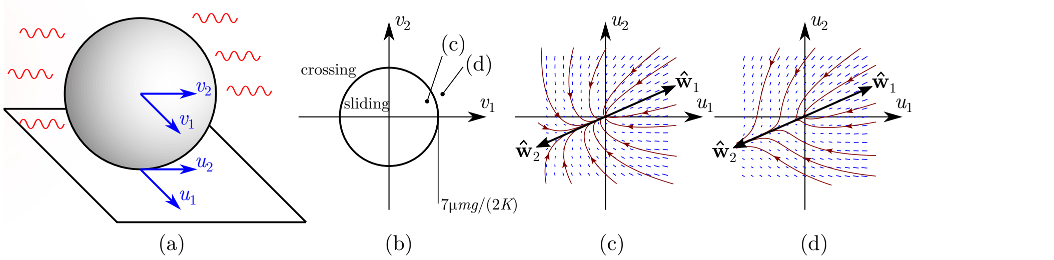

FIGURE 8. *Model of a ball slipping on a plane in a viscous medium.* (a) *Sketch of the model with the state variables of the system.* (b) *Sliding and crossing regions of the discontinuity set* $\Sigma \ni \mathbf{x}_t = (0, 0, v_1, v_2)$*.* (c)*,* (d) *Dynamics of the normal variables* $\mathbf{x}_o = (u_1, u_2, 0, 0)$ *at the discontinuity set in the sliding and crossing regions, respectively.*

The codimension-2 discontinuity set is $u_1 = u_2 = 0$; the orthogonal and tangential parts of the state variable are $\mathbf{x}_o = (u_1, u_2, 0, 0)$ and $\mathbf{x}_t = (0, 0, v_1, v_2)$, respectively. The polar decomposition becomes $r = \sqrt{u_1^2 + u_2^2}$ and $\mathbf{w} = (u_1/\sqrt{u_1^2 + u_2^2}, u_2/\sqrt{u_1^2 + u_2^2})$. From the calculation steps shown in the previous examples, we can show that there are always two limit directions, $\hat{\mathbf{w}}_{1,2} = \pm(v_1/\sqrt{v_1^2 + v_2^2}, v_2/\sqrt{v_1^2 + v_2^2})$, which are parallel to the velocity of the center of gravity of the ball. The direction $\hat{\mathbf{w}}_1$ is always attracting-isolated. The direction $\hat{\mathbf{w}}_2$ is attracting-dominant for $\sqrt{v_1^2 + v_2^2} < 7\mu mg/(2K)$ (Figure 8(c)) and it is repelling-isolated for $\sqrt{v_1^2 + v_2^2} > 7\mu mg/(2K)$ (Figure 8(d)). Thus, on the plane (v_1, v_2) of the tangential variable $\mathbf{x}_t$, the sliding and crossing regions are separated by the circle $\sqrt{v_1^2 + v_2^2} = 7\mu mg/(2K)$ (see Figure 8(b)). Outside this circle, being in the crossing region means that the *roll* motion of the ball is not realizable. Inside the circle, being in the sliding region means that the ball is capable of sustained roll motion.

Next, we determine the sliding dynamics in the sliding region and its mechanical meaning. At $u_1 = u_2 = 0$, the limit vector field $\mathbf{F}^\star$ can be put into the form (5.5)–(5.6), where $\mathbf{b} = \mathbf{w}$, and the matrices become

$$\mathbf{A}_o = \begin{pmatrix} -\frac{7}{2}\mu g & 0 \\ 0 & -\frac{7}{2}\mu g \end{pmatrix}, \qquad \mathbf{A}_t = \begin{pmatrix} -\mu g & 0 \\ 0 & -\mu g \end{pmatrix}, \qquad \mathbf{c}_o = \mathbf{c}_t = \begin{pmatrix} -\frac{K}{m} v_1 \\ -\frac{K}{m} v_2 \end{pmatrix}. \tag{5.12}$$

By using the formula (5.7), the sliding dynamics becomes

$$\tilde{\mathbf{F}} = \begin{pmatrix} 0 \\ 0 \\ -\frac{5}{7}\frac{K}{m} v_1 \\ -\frac{5}{7}\frac{K}{m} v_2 \end{pmatrix}. \tag{5.13}$$

It can be checked that (5.13) recovers correctly the differential equations of the *rolling* ball, which can be derived by the Newton–Euler equations considering the rolling *constraint* $u_1 = u_2 = 0$. This example demonstrates that in mechanical problems, the *sliding* dynamics corresponds to the local static mechanical state at the contact point (sticking or rolling). The mechanical *slipping* is described by the dynamics outside the discontinuity set.

6. Conclusion. Classical Filippov systems with codimension-1 discontinuity sets are natural descriptions of various natural phenomena. However, many simple models give rise to discontinuity sets of higher codimensions. For example, the one-dimensional motion of a rigid body under dry friction is modeled by a Filippov system; however, two-dimensional motion and motion under spinning frictional torque induce dynamics with codimension-2 and 3 discontinuities. The dynamics of systems with codimension-2 discontinuity was recently analyzed by [2], and in the present paper, we presented a similar analysis in the general case of codimension-n discontinuity sets.

In both cases, the dynamics in a small neighborhood of the discontinuity set is captured by decomposition of the vector field to radial, tangential, and circumferential components. The circumferential component is trivial in the case of Filippov systems. For $n = 2$, all important properties of the circumferential dynamics are captured by analyzing its fixed points (i.e., limit directions), with special attention for the case of missing limit directions. In contrast, the case of $n > 2$ may give rise to richer circumferential dynamics with convergence to various possible types of invariant sets ranging from fixed points to polycycles and strange attractors. We show how some of these give rise to pathological behavior, and thus we propose to exclude such systems from further analysis.

We make initial steps toward completing the discontinuous vector fields by defining sliding and crossing points as well as sliding dynamics along the discontinuity set. Similarly to the codimension-2 case, the uniqueness of the sliding vector field is not satisfied but by a restricted class of systems. Importantly, we find that models of friction-induced dynamics are consistent with these restrictions. Sliding dynamics represents the physical stick or roll motion at the contacts in this case.

Our analysis regarding dynamics at the discontinuity set remains incomplete. Most importantly, crossing points were characterized by the existence of concatenated trajectories crossing the discontinuity, whereas sliding points were characterized by the absence of such trajectories. We formulated the unproven conjecture that the sliding vector field exists for all sliding points. However, it should be noted that the sliding vector exists at some crossing points. In such a case, it is a subtle question, beyond the scope of this work, of which type of behavior is chosen by the system. There are even more types of nonuniqueness associated with crossing points: a crossing point can have multiple or even infinitely many outgoing trajectories, and any of them can be used as the continuation of an incoming trajectory. Resolving this type of nonuniqueness, analyzing bifurcation points from sliding to crossing as well as other types of transition points are among the questions left for future work. We also expect that deeper analysis will uncover further peculiar behavior in analogy with the known singularities of Filippov systems associated with tangencies.

REFERENCES

[1] M. Antali and G. Stepan, *Discontinuity-induced bifurcations of a dual-point contact ball*, Nonlinear Dynam., 83 (2016), pp. 685–702, https://doi.org/10.1007/s11071-015-2356-y.

[2] M. Antali and G. Stepan, *Sliding and crossing dynamics in extended Filippov systems*, SIAM J. Appl. Dyn. Syst., 17 (2018), pp. 823–858, https://doi.org/10.1137/17M1110328.

[3] M. Antali and G. Stepan, *Nonsmooth analysis of three-dimensional slipping and rolling in the presence of dry friction*, Nonlinear Dynam., 97 (2019), pp. 1799–1817, https://doi.org/10.1007/s11071-019-04913-x.

[4] J. A. Batlle, *The sliding velocity flow of rough collisions in multibody systems*, J. Appl. Mech., 63 (1996), pp. 804–809, https://doi.org/10.1115/1.2823366.
[5] A. P. da Costa and A. Seeger, *Cone-constrained eigenvalue problems: Theory and algorithms*, Comput. Optim. Appl., 45 (2010), pp. 25–57, https://doi.org/10.1007/s10589-008-9167-8.
[6] P. R. da Silva, I. S. Meza-Sarmiento, and D. D. Novaes, *Nonlinear sliding of discontinuous vector fields and singular perturbation*, Differ. Equ. Dyn. Syst., (2018), https://doi.org/10.1007/s12591-018-0439-1.
[7] M. di Bernardo, C. J. Budd, A. R. Champneys, and P. Kowalczyk, *Piecewise-Smooth Dynamical Systems*, Springer, New York, 2008.
[8] L. Dieci and L. Lopez, *Sliding motion on discontinuity surfaces of high co-dimension. A construction for selecting a Filippov vector field*, Numer. Math., 117 (2011), pp. 779–811, https://doi.org/10.1007/s00211-011-0365-4.
[9] M. Farkas, *Periodic Motions*, Appl. Math. Sci. 104, Springer, New York, 1994.
[10] N. Fenichel, *Geometric singular perturbation theory for ordinary differential equa tions*, J. Differential Equations, 31 (1979), pp. 53–98, https://doi.org/10.1016/0022-0396(79)90152-9.
[11] A. F. Filippov, *Differential Equations with Discontinuous Righthand Sides*, Kluwer, Dordrecht, 1988.
[12] A. Gaunersdorfer, *Time averages for heteroclinic attractors*, SIAM J. Appl. Math., 52 (1992), pp. 1476–1489, https://doi.org/10.1137/0152085.
[13] C. Glocker, *Set-Valued Force Laws*, Springer, New York, 2001.
[14] J. Guckenheimer and P. Holmes, *Nonlinear Oscillations, Dynamical Systems, and Bifurcations of Vector Fields*, Appl. Math. Sci. 42, Springer, New York, 2013.
[15] G. Hardy, J. Littlewood, and G. Polya, *Inequalities*, Cambridge University Press, Cambridge, UK, 1952.
[16] M. R. Jeffrey, *Dynamics at a switching intersection: Hierarchy, isonomy, and multiple sliding*, SIAM J. Appl. Dyn. Syst., 13 (2015), pp. 1082–1105, https://doi.org/10.1137/13093368X.
[17] M. R. Jeffrey, *Hidden Dynamics*, Springer, New York, 2018.
[18] K. L. Johnson, *Contact Mechanics*, Cambridge University Press, Cambridge, UK, 1985.
[19] P. Kaklamanos and K. U. Kristiansen, *Regularization and geometry of piecewise smooth systems with intersecting discontinuity yets*, SIAM J. Appl. Dyn. Syst., 18 (2019), pp. 1225–1264, https://doi.org/10.1137/18M1214470.
[20] K. U. Kristiansen and S. J. Hogan, *On the use of blowup to study regularizations of singularities of piecewise smooth dynamical systems in* $\mathbb{R}^3$, SIAM J. Appl. Dyn. Syst., 14 (2015), pp. 382–422, https://doi.org/10.1137/140980995.
[21] G. Kudra and J. Awrejcewicz, *Tangens hyperbolicus approximations of the spatial model of friction coupled with rolling resistance*, Internat. J. Bifur. Chaos, 21 (2011), pp. 2905–2917, https://doi.org/10.1142/S0218127411030222.
[22] C. Kuehn, *Multiple Time Scale Dynamics*, Springer, New York, 2015.
[23] R. I. Leine and C. Glocker, *A set-valued force law for spatial Coulomb–Contensou friction*, Eur. J. Mech. A Solids, 22 (2003), pp. 193–216, https://doi.org/10.1016/S0997-7538(03)00025-1.
[24] R. I. Leine and H. Nijmeijer, *Dynamics and Bifurcations of Non-Smooth Mechanical Systems*, Springer, New York, 2004.
[25] J. Libre, P. R. da Silva, and M. A. Teixeira, *Regularization of discontinuous vector fields on* $\mathbb{R}^3$ *via singular perturbation*, J. Dynam. Differential Equations, 19 (2007), pp. 309–331, https://doi.org/10.1007/s10884-006-9057-7.
[26] J. Llibre, P. da Silva, and M. A. Teixeira, *Sliding vector fields for non-smooth dynamical systems having intersecting switching manifolds*, Nonlinearity, 28 (2015), pp. 493–507, https://doi.org/10.1088/0951-7715/28/2/493.
[27] V. J. Lopez and J. Llibre, *A topological characterization of the ω-limit sets for analytic flows on the plane, the sphere and the projective plane*, Adv. Math., 216 (2007), pp. 677–710, https://doi.org/10.3934/dcdsb.2019010.
[28] E. Magyari and P. Weidman, *Frictionally coupled sliding and spinning on an inclined plane*, Phys. D, 413 (2020), 132647, https://doi.org/10.1016/j.physd.2020.132647.
[29] D. D. Novaes and M. R. Jeffrey, *Regularization of hidden dynamics in piecewise smooth flows*, J. Differential Equations, 259 (2015), pp. 4615–4633, https://doi.org/10.1016/j.jde.2015.06.005.

[30] D. Panazzolo and P. R. da Silva, *Regularization of discontinuous foliations: Blowing up and sliding conditions via Fenichel theory*, J. Differential Equations, 263 (2017), pp. 8362–8390, https://doi.org/10.1016/j.jde.2017.08.042.

[31] K. Sigmund, *Time averages for unpredictable orbits of deterministic systems*, Ann. Oper. Res., 37 (1992), pp. 217–228, https://doi.org/10.1007/BF02071057.

[32] J. Sotomayor and M. A. Teixeira, *Regularization of discontinuous vector fields*, in Proceedings of the International Conference on Differential Equations, Lisboa, Equadiff 95, 1996, pp. 207–223.

[33] M. A. Teixeira, *Generic singularities of discontinuous vector fields*, An. Acad. Brasil. Ciênc., 53 (1981), pp. 257–260.

[34] M. A. Teixeira, *Generic bifurcation of sliding vector fields*, J. Math. Anal. Appl., 176 (1993), pp. 436–457, https://doi.org/10.1006/jmaa.1993.1226.

[35] V. I. Utkin, Springer, New York, 1992.

[36] F. Verhulst, *Methods and Applications of Singular Perturbations: Boundary Layers and Multiple Timescale Dynamics*, Springer, New York, 2005.

[37] S. Walker and R. I. Leine, *Set-valued anisotropic dry friction laws: Formulation, experimental verification and instability phenomenon*, Nonlinear Dynam., 96 (2019), pp. 885–920, https://doi.org/10.1007/s11071-019-04829-6.